Article

Molecular Cell

A Slow Conformational Switch in the BMAL1 Transactivation Domain Modulates Circadian Rhythms

Graphical Abstract

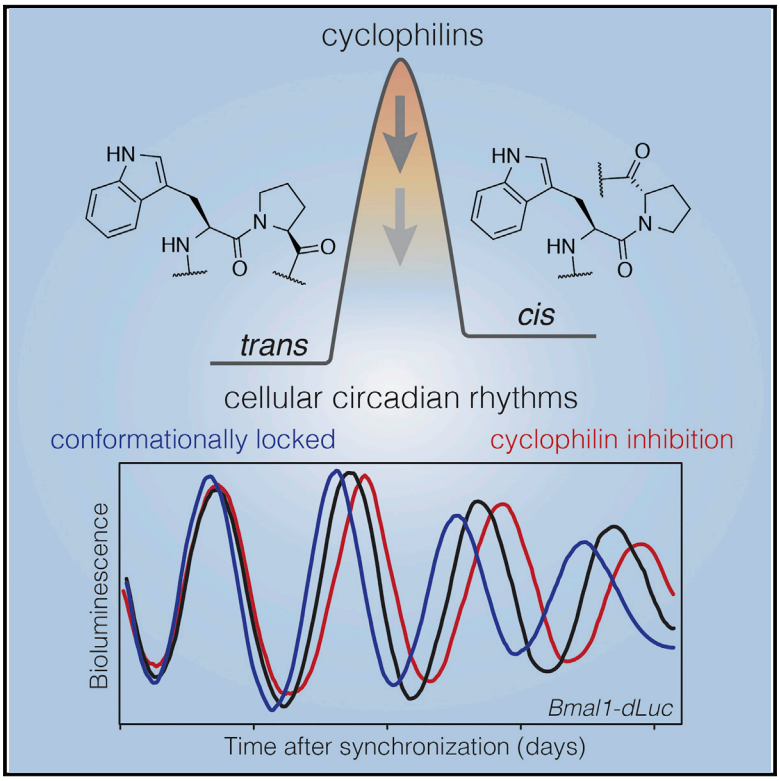

Authors

Chelsea L. Gustafson, Nicole C. Parsley, Hande Asimgil, ..., Tara L. Davis, Andrew C. Liu, Carrie L. Partch

Correspondence

cpartch@ucsc.edu

In Brief

Gustafson et al. identify a *cis/trans* isomerization switch in the BMAL1 transactivation domain that controls circadian rhythms. Conformationally locking the switch or inhibiting prolyl isomerases influences circadian period to suggest that slow protein dynamics play a role in timekeeping.

Highlights

- The highly flexible BMAL1 TAD possesses a slow binary conformational switch
- The switch is generated by *cis/trans* isomerization about a Trp-Pro imide bond
- Conformationally locking the switch into *trans* isomer shortens circadian period
- Cyclophilins accelerate isomerization to modulate circadian period

Gustafson et al., 2017, Molecular Cell *66*, 447–457
May 18, 2017
http://dx.doi.org/10.1016/j.molcel.2017.04.011

CellPress

Molecular Cell
Article

A Slow Conformational Switch in the BMAL1 Transactivation Domain Modulates Circadian Rhythms

Chelsea L. Gustafson,[1,6] Nicole C. Parsley,[1] Hande Asimgil,[1] Hsiau-Wei Lee,[1] Christopher Ahlbach,[1] Alicia K. Michael,[1] Haiyan Xu,[2] Owen L. Williams,[1] Tara L. Davis,[3] Andrew C. Liu,[2,4] and Carrie L. Partch[1,5,7,*]
[1]Department of Chemistry and Biochemistry, University of California, Santa Cruz, Santa Cruz, CA 95064, USA
[2]Department of Biological Sciences, University of Memphis, Memphis, TN 38152, USA
[3]Department of Biochemistry and Molecular Biology, Drexel University College of Medicine, Philadelphia, PA 19104, USA
[4]Feinstone Genome Research Center, University of Memphis, Memphis, TN 38152, USA
[5]Center for Circadian Biology, University of California, San Diego, San Diego, CA 92093, USA
[6]Present address: Department of Natural Sciences, Oregon Institute of Technology, Wilsonville, OR 97070, USA
[7]Lead Contact
*Correspondence: cpartch@ucsc.edu
http://dx.doi.org/10.1016/j.molcel.2017.04.011

SUMMARY

The C-terminal transactivation domain (TAD) of BMAL1 (brain and muscle ARNT-like 1) is a regulatory hub for transcriptional coactivators and repressors that compete for binding and, consequently, contributes to period determination of the mammalian circadian clock. Here, we report the discovery of two distinct conformational states that slowly exchange within the dynamic TAD to control timing. This binary switch results from *cis/trans* isomerization about a highly conserved Trp-Pro imide bond in a region of the TAD that is required for normal circadian timekeeping. Both *cis* and *trans* isomers interact with transcriptional regulators, suggesting that isomerization could serve a role in assembling regulatory complexes in vivo. Toward this end, we show that locking the switch into the *trans* isomer leads to shortened circadian periods. Furthermore, isomerization is regulated by the cyclophilin family of peptidyl-prolyl isomerases, highlighting the potential for regulation of BMAL1 protein dynamics in period determination.

INTRODUCTION

Mammalian circadian clocks are intrinsic molecular timekeeping systems that coordinate physiological processes with external environmental cues in order to appropriately time daily activities. This coordination is achieved by two interlocked transcription feedback loops that control the temporal basis of expression for over 40% of the mammalian genome (Zhang et al., 2014). The heterodimeric transcription factor CLOCK:BMAL1 sits at the core of the primary feedback loop that directs the chronometric transcription of clock-controlled genes. Circadian timekeeping is established through the coordinate regulation of CLOCK:BMAL1 by transcriptional coactivators, such as CBP/p300, and the dedicated circadian repressors PER and CRY (Partch et al., 2014). Many processes contribute to the timing of activation and repression, such as the localization, phosphorylation, and degradation of repressors in the nucleus (reviewed in Gallego and Virshup, 2007). However, the mechanisms that regulate the changing architecture of CLOCK:BMAL1 transcriptional regulatory complexes throughout the day are still poorly understood (Koike et al., 2012). The highly dynamic BMAL1 (brain and muscle ARNT-like 1) transactivation domain (TAD) is one hub for these interactions, as it interacts with both coactivators and repressors and is necessary for circadian oscillations (Kiyohara et al., 2006; Park et al., 2015; Xu et al., 2015). Modulating affinity of the BMAL1 TAD for its regulators elicits large changes in period, demonstrating an important role in timekeeping of the transcription-based clock (Xu et al., 2015). Identification of processes that fine-tune interactions between the BMAL1 TAD and transcriptional regulators will shed light on the mechanism by which animals measure time and use it to coordinate behavior and physiology with the environment.

By inducing changes in conformation, protein-protein interactions, or subcellular localization, post-translational modifications play critical roles in controlling signaling pathways and information processing. Additionally, proteins exhibit a range of dynamic behaviors on different timescales that can also contribute to functional output (Henzler-Wildman and Kern, 2007). From the fast, stochastic motions of intrinsically disordered regions to the longer timescales of coordinated domain motions and protein folding, the dynamic behavior of proteins ultimately governs how they regulate biological processes. One such behavior is conformational *cis/trans* isomerization about a proline-containing imide peptide bond (Xaa-Pro); popularly dubbed a "molecular timer" (Lu et al., 2007), isomerization is an intrinsically slow process (from milliseconds to minutes) that can be enzymatically accelerated by peptidyl prolyl isomerases (PPIases) by up to ~4–5 orders of magnitude (Schmid, 1993). Proline isomerization is relatively rare, as only ~6% of imide bonds are estimated

to undergo isomerization (Stewart et al., 1990), but it has a profound impact on diverse cellular processes, such as transcription (Bataille et al., 2012; Nelson et al., 2006), protein folding (Wedemeyer et al., 2002), ion channel gating (Lummis et al., 2005), and protein degradation (Liou et al., 2011). Likewise, proline isomerases are pivotal components of many intracellular signaling pathways through their acceleration of this otherwise slow process (Brazin et al., 2002; Lang et al., 1987; Saleh et al., 2016). Dysfunctional regulation of proline isomerization and/or PPIase activity has been implicated in cancer (Zhou and Lu, 2016), Alzheimer's disease (Nakamura et al., 2012), and regulation of circadian rhythms in *Drosophila* (Kang et al., 2015).

Here, we report the discovery of a slow conformational switch in the BMAL1 TAD that modulates mammalian circadian rhythms. Using nuclear magnetic resonance (NMR) spectroscopy, we show that *cis*/*trans* isomerization about a conserved Trp-Pro imide bond generates this conformational exchange, which we have dubbed the "TAD switch." To study the roles of individual isomers in interactions with circadian transcriptional regulators, we developed locked *cis* and *trans* isomers using site-directed mutagenesis or peptide synthesis with unnatural amino acids. Locked isomers bind CRY1 and CBP KIX with similar affinities, yet locking the TAD into its *trans* isomer shortens the circadian period in cell-based assays, demonstrating that exchange between these two conformations contributes to circadian timekeeping. Using NMR, we determined that the timescale of isomerization is intrinsically slow, taking minutes to complete a cycle of exchange. We then identified a group of PPIases within the cyclophilin family that significantly enhance rates of isomerization. Inhibition of cyclophilins lengthens the circadian period in a switch-dependent manner, suggesting that enzymatic modulation of intrinsically slow dynamics at the BMAL1 TAD could play a role in tuning the circadian period in vivo.

RESULTS

Proline Isomerization Acts as a Molecular Switch in the C Terminus of BMAL1

The BMAL1 TAD acts as a regulatory hub that interacts with positive or negative transcriptional regulators as a function of circadian time (CT) to control the activation state of CLOCK:BMAL1 (Koike et al., 2012). We previously used NMR spectroscopy to identify overlapping binding sites of the transcriptional coactivator CBP/p300 and the repressor CRY that map to two distinct sites in the BMAL1 TAD: the predicted alpha helical region in the center of the TAD and the extreme C terminus (Figure 1A) (Xu et al., 2015). ^{15}N-^{1}H heteronuclear single quantum coherence (HSQC) NMR spectra display a peak for each of the constituent N-H bonds in the disordered TAD. The chemical shift, or location of the peaks, represents a population-weighted average of conformations that interconvert in fast exchange. To our surprise, the ^{15}N-^{1}H HSQC spectrum of the BMAL1 TAD revealed two distinct resonances for each of the eight C-terminal residues (Figures 1B and S1A), indicating slow exchange between two conformations localized to this distal site. We performed liquid chromatography/mass spectrometry analysis on the ^{15}N-labeled NMR sample, which demonstrated the presence of a single, highly pure peptide of the expected molecular weight (Figures S1B and S1C). Moreover, truncation of the C-terminal seven residues resulted in a ^{15}N-^{1}H HSQC spectrum devoid of peak doubling, confirming that chemical exchange requires the extreme C terminus of the TAD (Figure S1A).

To identify the structural basis for this conformational heterogeneity, we turned to the C(CO)NH TOCSY (total correlated spectroscopy) NMR experiment, which correlates side chain carbon chemical shifts with the following amide peptide bond to provide sequence-specific information about the local environment. Looking back from the doubled amide peaks for residue L626, the chemical shifts of P625 $^{13}C_{\beta}$ and $^{13}C_{\gamma}$ atoms unambiguously identified that the W624-P625 imide bond is found in two distinct conformations, a *cis* form and a *trans* form based on a comparison to NMR chemical shift databases (Figures 1C and 1D) (Shen and Bax, 2010). No *cis* isomer was detected for P623 or any of the other three imide bonds in the BMAL1 TAD construct (Figures 1C and S1D–S1F), demonstrating that peak doubling in the C terminus is due solely to slow isomerization of the Trp-Pro bond. Using the relative abundance of several representative peaks of the two isomers, we determined that the population of the TAD switch under these conditions is approximately 65% *trans* and 35% *cis* isomers (Figure S1G).

Conservation of the TAD Switch from Insects to Vertebrates

To begin exploring the functional significance of the TAD switch, we first examined its conservation across BMAL orthologs (Figure 1E). We noted that the proline of the switch is not conserved in vertebrate BMAL2, a homolog of BMAL1 that has an active TAD but cannot sustain circadian cycling outside of the suprachiasmatic nucleus (Shi et al., 2010; Xu et al., 2015). Phylogenetic analysis of CYCLE, the insect ortholog of BMAL1, demonstrates its divergence into two distinct gene families: a *Drosophila*-like CYCLE (dCYC) that possesses only the N-terminal bHLH (basic-helix-loop-helix), PAS-A, and PAS-B domains, and a vertebrate BMAL1-like CYCLE that also contains the C-terminal TAD (Chang et al., 2003). The BMAL1-like CYCLE genes found in insects also possess a vertebrate-like cryptochrome with transcriptional repressor activity, suggesting that the network architecture of these molecular clocks is similar to that of vertebrates (Rubin et al., 2006; Zhu et al., 2008). Because these insect CYC genes exhibit higher functional and structural homology to vertebrate BMAL1 than *Drosophila* CYC, we hereinafter refer to these genes as insect-BMAL1 (iBMAL1). We found that the TAD switch is strictly conserved in all iBMAL1 genes, indicating that the presence of the switch in BMAL1 predates the divergence of insects and vertebrates about 600 million years ago (Peterson et al., 2004).

Although the eight residues of the BMAL1 TAD switch are highly conserved throughout metazoans, we noted several substitutions upstream of the conserved Trp-Pro switch and the inclusion of an additional C-terminal proline in some invertebrates (Figure 1E). To determine whether these sequence variations affect the switch, we synthesized 8-mer peptides using the vertebrate BMAL1 and *Apis florea* iBMAL1 sequences and

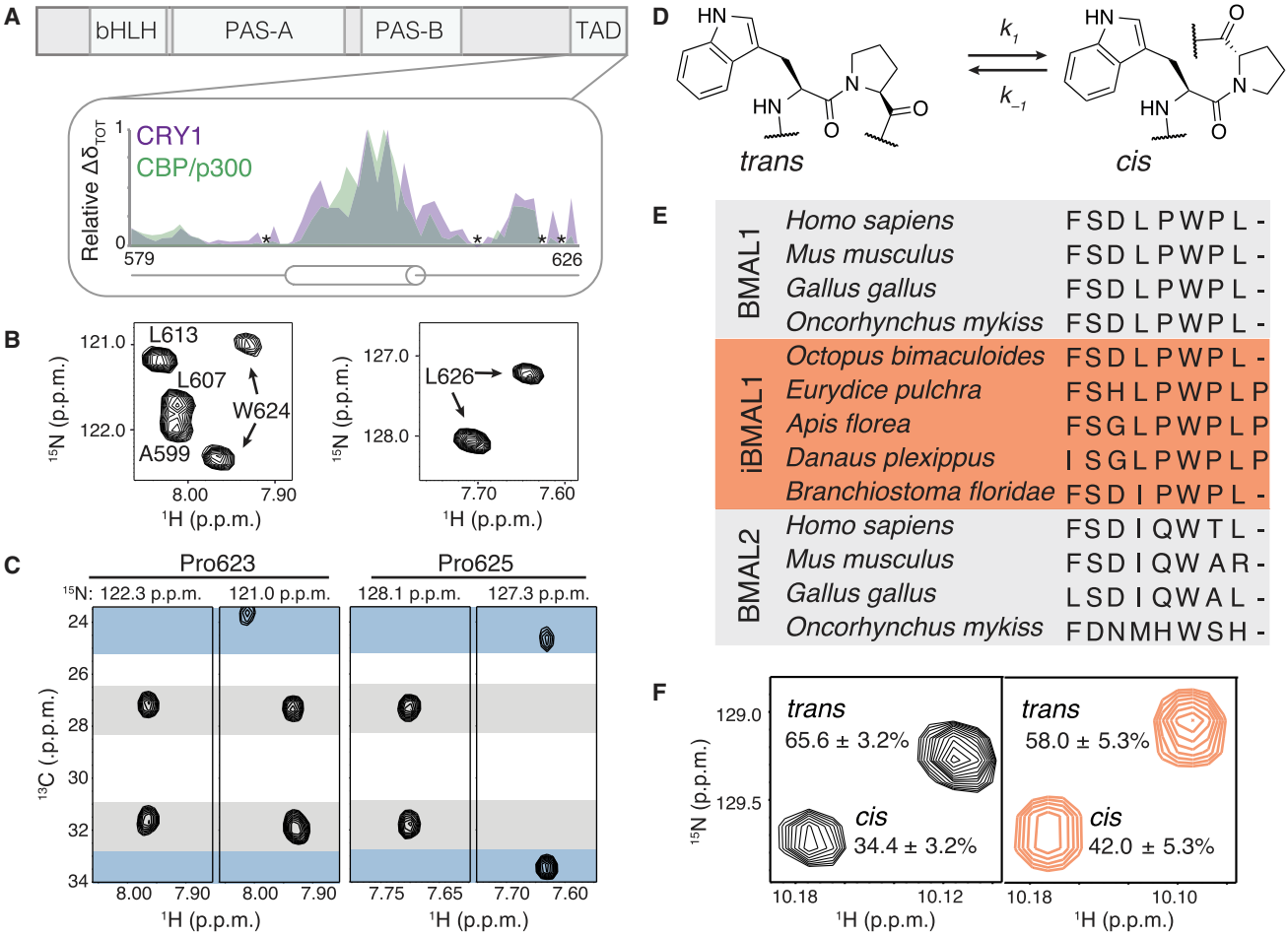

Figure 1. Isomerization about a Conserved Trp-Pro Imide Bond in the BMAL1 C-Terminal TAD

(A) Domain schematic of mouse BMAL1 showing the chemical shifts (Δδ) in the TAD after binding the CRY1 CC helix (purple) or CBP KIX domain (green). Asterisk indicates proline residues that lack crosspeaks in ^{15}N-^{1}H HSQC NMR spectra.

(B) Selected regions of ^{15}N-^{1}H HSQC spectra of ^{15}N BMAL1 TAD displaying backbone amide peaks for two isomers at W624 and L626. p.p.m., parts per million.

(C) Crosspeaks for P623 and P625 C_β and C_γ atoms are shown in strips from the ^{15}N-edited (H)C(CO)NH TOCSY of ^{13}C/^{15}N BMAL1 TAD at ^{15}N planes for W624 and L626 amides. Average ^{13}C shifts for *trans* (gray) and *cis* (blue) isomers from (Shen and Bax, 2010).

(D) The W624-P625 imide bond in *cis* and *trans* conformations.

(E) Sequence alignment BMAL1, BMAL2, and CYCLE from insects with a vertebrate-like clock (iBMAL1).

(F) Regions of ^{15}N-^{1}H HSQC spectra of 8-mer switch peptides from mouse (FSDLPWPL, black) and dwarf honeybee (FSGLPWPLP, peach) showing *cis* and *trans* peaks for W624 indole.

See also Figure S1.

analyzed peak intensities from ^{15}N-^{1}H HSQC spectra collected on natural abundance samples. The vertebrate switch peptide (FSDLPWPL) displayed an equilibrium population of isomers similar to that of the intact mouse BMAL1 TAD (Figures 1F, S1G, and S1H), as did the iBMAL1 switch peptide (FSGLPWPLP) (Figure 1F), suggesting that insects with a vertebrate-like clock likely share switch functionality with mouse BMAL1.

TRP and PRO Are the Key Residues that Constitute the TAD Switch

To probe the importance of the two switch isomers for circadian rhythms, we first set out to identify local sequence requirements that contribute to the TAD switch. By carefully defining these local factors in vitro, we aimed to validate a set of molecular tools that would allow us to explore switch function in the cellular environment. With rare exception, only proline allows the *cis* isomer to arise in a peptide bond (Pal and Chakrabarti, 1999). As expected, the mutation of P625 to Ala eliminated detection of the *cis* isomer by NMR, providing us with a *trans*-locked BMAL1 (Figures 2A and 2B). Conversely, integration of the bulky analog 5,5-dimethyl proline (dmP) (Lummis et al., 2005; Nakamura et al., 2012) in place of P625 produced the opposite effect, a TAD switch exclusively populating the *cis* isomer (Figures 2A and 2B). The backbone geometry of these mutants was verified using ^{13}C-^{1}H HSQC and ^{1}H-^{1}H TOCSY spectra collected on natural abundance peptides (Figures S2A and S2B). The P625A *trans*-locked

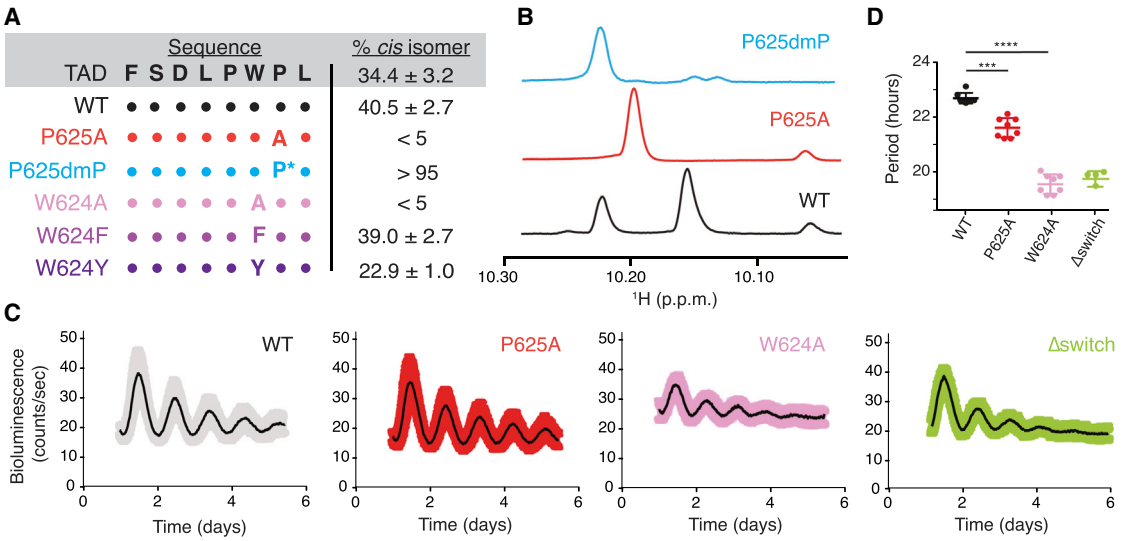

Figure 2. Locked Mutants of the TAD Switch Shorten the Circadian Period

(A) Representation of *cis* content of 8-mer TAD switch peptides for P625 and W624 mutants compared to the intact ^{15}N BMAL1 TAD. The *cis* content was calculated from peak volumes of residues 624 and 626 in ^{15}N-^{1}H HSQC and ^{1}H-^{1}H TOCSY NMR spectra. WT, wild-type.

(B) ^{1}H NMR spectra from FSDLPWPL (black), FSDLPWAL (red), and FSDLPWdmPL (blue) 8-mer TAD switch peptides highlighting the W624 indole region.

(C) Synchronized circadian bioluminescence records from *Bmal1*$^{-/-}$;*Per2*^{Luc} mouse fibroblasts complemented with WT (gray), W624A (pink), P625A (red), or Δswitch (619X, green) *Bmal1*. Black line indicates mean luminescence ± SD from n = 6–8 replicates from two independent clonal lines in indicated colors.

(D) Circadian period of complemented fibroblast lines from (C). Individual period measurements with mean ± SD. ***p < 0.01; ****p < 0.0001, compared to WT *Bmal1* by two-tailed t test.

See also Figure S2.

switch mutant was also incorporated into the intact BMAL1 TAD (residues 579–626) to establish that *cis*/*trans* isomer ratios were found to be similar by NMR spectroscopy (Figure S2C).

Long-range interactions affecting the equilibrium population of *cis*/*trans* isomers have been reported in some highly structured systems (Wedemeyer et al., 2002), but for intrinsically disordered regions such as the BMAL1 TAD, long-range constraints are unlikely to affect isomerization (Theillet et al., 2014). By contrast, the identity of the (*i-1*) residue that precedes proline has a profound impact on the equilibrium population of *cis* isomers. Aromatic amino acids in the (*i-1*) position increase the propensity of an imide bond to sample the *cis* conformation through stabilizing interactions of the π aromatic face with the proline C-H_α bond (Zondlo, 2013), while small, electron-poor amino acids typically decrease the stability of the *cis* isomer (Reimer et al., 1998; Shen and Bax, 2010). As predicted, the replacement of W624 with Ala resulted in no observable *cis* isomer population in both the 8-mer peptide and the intact TAD (Figures 2A, 2B, and S2A–S2C). Likewise, decreasing the aromaticity of the (*i-1*) residue by substitution of W624 with Tyr resulted in a decrease in the *cis* population (Figures 2A, S2A, and S2B). Altogether, these data demonstrate that both Trp and Pro residues are important for the observed conformational switch in the BMAL1 TAD.

The *trans*-Locked TAD Switch Drives Shortened Circadian Rhythms

Mutations in the BMAL1 TAD elicit control over the period of the transcription-based clock by differentially regulating affinity for transcriptional coactivators and repressors. For example, substitution of two key residues in the central alpha helical region of the TAD (L606A/L607A) disrupted circadian rhythms altogether by eliminating interactions with regulators, while other mutations led to circadian periods ranging from ~19 to 26 hr; notably, deletion of the last seven residues of the TAD (619X, referred to as Δswitch here) shortened the intrinsic period by approximately 3 hr (Xu et al., 2015). To examine the functional consequences of disrupting the TAD switch on circadian rhythms, we stably incorporated different *trans*-locked *Bmal1* mutants into *Bmal1*$^{-/-}$;*Per2*^{Luc} cells. In our hands, complementation with wild-type *Bmal1* resulted in a period of approximately 23 hr (Figures 2C, 2D, S2D, and S2E), while the P625A mutant decreased this period by over 1 hr. Complementation with W624A *Bmal1* led to an ~3 hr decrease in period, on par with the shortened period observed on deletion of the entire switch region (Figures 2C, 2D, S2D, and S2E) (Xu et al., 2015). Moreover, the W624A/P625A double mutant exhibited a short period in a manner similar to that of the W624A mutant (Figures S2D and S2E), demonstrating that, while locking the switch into the *trans* isomer has a significant effect on period, this effect is further enhanced by deletion of the bulky aromatic side chain of W624.

Both Isomers of the TAD Switch Interact with Transcriptional Regulators

To begin to probe the molecular mechanism for the short period phenotype observed upon complementation with *trans*-locked mutants of *Bmal1*, we quantitatively analyzed the interaction of

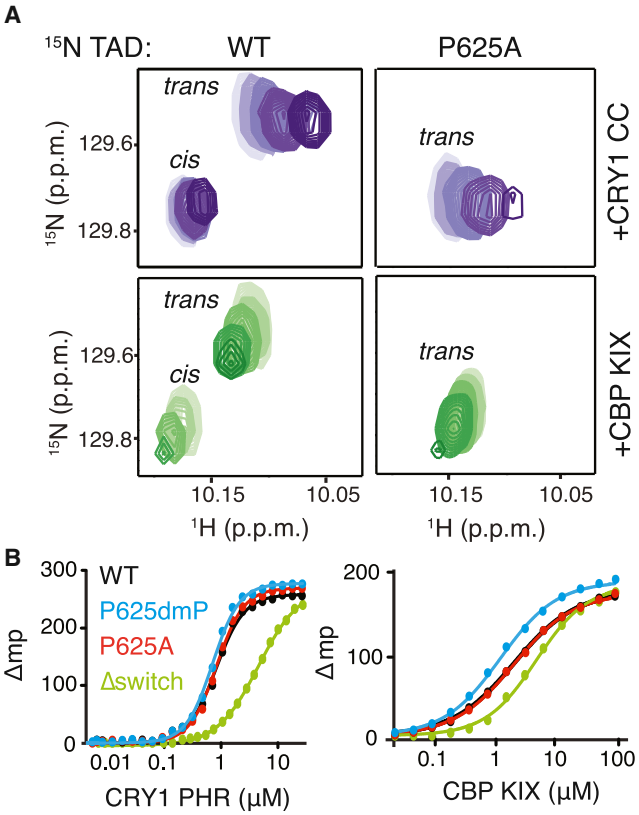

Figure 3. Both Isomers of the TAD Switch Interact with Transcriptional Activators and Repressors

(A) Regions of the ^{15}N-^{1}H HSQC spectra showing 100 μM WT (left panels) or P625A (right panels) ^{15}N BMAL1 TAD upon titration of CRY1 CC (purple) or CBP KIX (green), with increasing concentrations from 25 μM to 200 μM indicated by darker colors. p.p.m., parts per million.

(B) Fluorescence anisotropy data for CRY1 PHR (left) and CBP KIX (right) with WT (black), P625A (red), P625dmP (blue), and Δswitch (green) 5,6-TAMRA-labeled short BMAL1 TAD (residues 594–626). Mean polarization data from one representative experiment (n = 4 replicates) of three independent assays. See also Figure S3.

cis and *trans* isomers of the TAD with known transcriptional regulators using NMR and fluorescence anisotropy. NMR studies performed on the wild-type ^{15}N BMAL1 TAD demonstrated that the CC helix and KIX domains of regulators CRY1 and CBP, respectively, each interact with both isomers present in the native TAD (Figure 3A, left panels). The same ^{15}N-^{1}H HSQC titration experiment was also performed on the *trans*-locked ^{15}N BMAL1 TAD P625A mutant, giving rise to chemical shift changes that were highly similar to those of the native *trans* isomer (Figure 3A, right panels; Figures S3A–S3C), suggesting that the P625A mutant is a reasonable proxy for the native *trans* isomer of the TAD.

We then determined affinities of locked variants of the TAD switch for CRY1 and the CBP KIX domain using fluorescence anisotropy with short labeled BMAL1 TAD peptides encompassing the highly conserved region from residues 594–626 (Xu et al., 2015). To promote robust changes in fluorescence polarization from the short TADs, we elected to use the ~50-kDa

Table 1. Affinity of BMAL1 TAD Mutants and Conformationally Locked Isomers for Transcriptional Regulators

	CRY1 PHR		CBP KIX	
BMAL1 TAD	K_D, in Micromolar	Hill	K_D, in Micromolar	Hill
WT	0.90 ± 0.27	1.6 ± 0.1	1.34 ± 0.40	0.99 ± 0.13
P625A	0.99 ± 0.27	1.8 ± 0.1	1.59 ± 0.66	0.98 ± 0.28
P625dmP	0.86 ± 0.17	1.9 ± 0.1	1.16 ± 0.44	1.02 ± 0.48
Δswitch	4.28 ± 0.33	0.9 ± 0.04	4.63 ± 1.05	0.91 ± 0.19

Data were acquired by fluorescence polarization assay and fit to a one-site binding model with Prism 6.0. Values shown are averages of three or four independent experiments ± SD; n = 2 or 3 replicates each. K_D, dissociation constant.

CRY1 photolyase homology region (PHR) that contains the CC helix instead of the isolated CC peptide because it has a similar affinity for the TAD (Czarna et al., 2013; Xu et al., 2015). In this assay, both wild-type (WT) and Δswitch TADs bound the CRY1 PHR and CBP KIX domain with affinities similar to those previously determined by isothermal titration calorimetry (Figure 3B; Table 1) (Czarna et al., 2013; Xu et al., 2015). Moreover, analysis of the CRY1 binding curve suggested positive cooperativity with a Hill coefficient of 1.6, possibly arising from enforced proximity effects (Ferrell and Cimprich, 2003; Pullen and Bolon, 2011) of the two CRY1 binding motifs at the central alpha helix and switch region of the TAD. In support of this, truncation of the switch region eliminated the apparent cooperativity (Table 1), further demonstrating its importance for interactions with regulators. However, binding assays with *cis*- and *trans*-locked short TADs demonstrated that affinities for the CRY1 PHR and CBP KIX domain were similar to those of WT (Figures 3B, S3D, and S3E; Table 1), indicating that the effects of the TAD switch on circadian period appear not to arise from differential affinity for either of the known binding partners under these conditions.

Isomerization of the TAD Switch Occurs on the Timescale of Minutes

The ability to switch between distinct protein conformations can regulate signaling by modulating affinity or occluding binding interfaces (Brazin et al., 2002; Sarkar et al., 2007), or by exerting kinetic control over isoenergetic conformational states to influence the selection of partners (Phillips et al., 2013). Isomerization about the imide bond is an inherently slow process, leading to experimentally determined rates of proline isomerization from milliseconds to nearly an hour in vitro (Eckert et al., 2005; Grathwohl and Wüthrich, 1981), considerably longer than the nanosecond backbone dynamics typically encountered in disordered proteins (Henzler-Wildman and Kern, 2007). To determine the timescale of exchange between *cis* and *trans* isomers in the BMAL1 TAD, we used ^{15}N-^{1}H ZZ-exchange NMR experiments that incorporate a short delay after encoding the ^{15}N frequency to capture interconversion via formation of crosspeaks that align with the ^{1}H frequency of the new state. When performed at 25°C, the absence of characteristic crosspeaks in the ^{15}N-^{1}H ZZ-exchange assay (Figure 4A) demonstrated

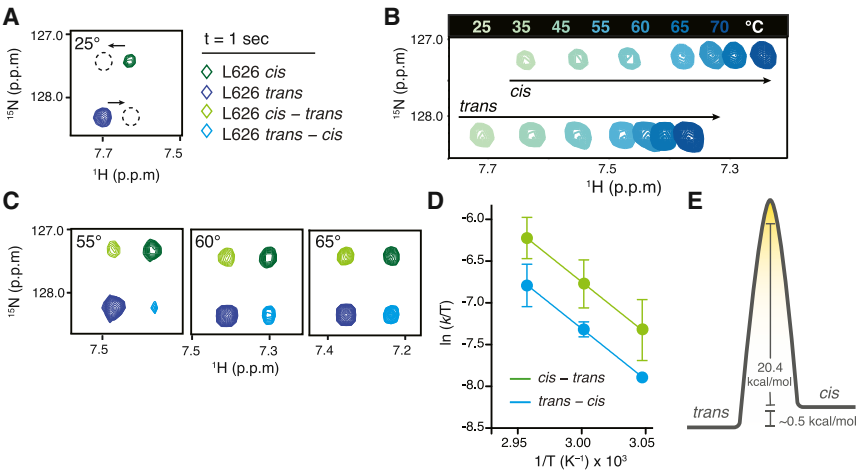

Figure 4. Slow Isomerization of the TAD Switch Occurs on the Timescale of Minutes

(A) Highlighted region of the 2D spectrum from a ^{15}N-^{1}H ZZ-exchange assay performed at 25°C of ^{15}N BMAL1 TAD displaying *cis* (dark green), *trans* (dark blue), *cis*-to-*trans* (light green), and *trans*-to-*cis* (light blue) crosspeaks for L626 at a delay = 1 s. Dashed circles indicate location of exchange crosspeaks. p.p.m., parts per million.

(B) Overlay of ^{15}N-^{1}H HSQC spectra showing the *cis* and *trans* peaks of L626 at increasing temperatures.

(C) Snapshot of ZZ-exchange assays at delay = 1 s at indicated temperatures.

(D) Eyring analysis of exchange rates versus temperature from ZZ-exchange assays, with errors displayed in SD.

(E) Free energy plot showing the calculated activation energy of isomerization for the BMAL1 TAD. See also Figure S4.

that isomerization was too slow to be detected at room temperature. Because intrinsically disordered proteins like the BMAL1 TAD already lack structural elements that are typically disrupted by high temperature, we increased the temperature to enhance isomerization rates. First, we collected a series of ^{15}N-^{1}H HSQC spectra at increasing temperatures up to 70°C (Figures 4B and S4A), observing that integrity of the BMAL1 TAD was retained after incubation at temperatures up to 70°C, with an essentially identical ^{15}N-^{1}H HSQC spectrum upon return to 25°C (Figure S4B), indicating no lasting effect of high temperature on the protein.

To explore the effect of temperature on switch kinetics, we collected ^{15}N-^{1}H ZZ-exchange datasets at increasing temperatures until we observed crosspeaks indicative of exchange. These crosspeaks first appeared at 55°C and grew in intensity with increasing temperature (Figure 4C). Intensities for peaks representing *cis* and *trans* isomers of the W624 side-chain indole and L626 backbone amide, as well as intensities for exchange crosspeaks, were extracted and plotted as a function of delay time (Figure S4C). Exchange rates were calculated independently for temperatures from 55°C to 65°C using the Bloch-McConnell equations (Farrow et al., 1994). We then plotted temperature-dependent exchange rates using the Eyring equation to extrapolate the kinetics of exchange to temperatures lower than 55°C (Figure 4C; Table 2). At 25°C, the time for *cis*-to-*trans* isomerization is calculated to take 3.64 min, while *trans*-to-*cis* isomerization takes 6.30 min, for an overall exchange lifetime of approximately 10 min. Based on these data, we calculated a barrier for *cis*/*trans* isomerization of ~20.4 kcal/mol, with a difference in stability between the two isomers of ~0.5 kcal/mol (Figure 4D), both on par with values for analogous systems (Reimer et al., 1998). Compared to the fast motions of the intrinsically disordered TAD backbone suggested by predominantly negative heteronuclear ^{15}N-^{1}H NOE (nuclear Overhauser effect) values (Figure S4D), slow isomerization of the Trp-Pro imide bond suggests that functionally relevant conformational dynamics may exist over at least 12 orders of magnitude in timescale in the BMAL1 TAD (Figure S4E).

Cyclophilins Can Accelerate Interconversion of the TAD Switch

Intrinsically slow rates of *cis*/*trans* isomerization are often enhanced catalytically by PPIases to regulate cellular signaling events. Notably, PPIases regulate circadian rhythms in *Drosophila*; however, activity of the Pin1-like Dodo isomerase is phosphoserine specific and appears to target PER proteins (Kang et al., 2015). Given that the BMAL1 TAD does not possess this phosphospecific consensus motif, we chose to focus our initial attention on cyclophilins for two reasons. First, the broadly expressed PPIase A (PPIA; also known as cyclophilin A [CypA]) co-immunoprecipitated with BMAL1 in a screen for interacting partners (Lipton et al., 2015); and second, the cyclophilin family has eight isoforms with nuclear localization (Adams et al., 2015) where, we believe, regulation of the TAD is likely to occur. To determine whether PPIA could regulate the TAD switch in vitro, we performed a ^{15}N-^{1}H ZZ-exchange NMR experiment on the BMAL1 TAD at room temperature in the presence of sub-stoichiometric concentrations of PPIA. As cyclophilins have notoriously low K_Ms (Michaelis-Menten constants; 0.3–1 mM) for their substrates (Coelmont et al., 2010; Schmid, 1993), this precluded a traditional analysis of the catalytic efficiency of PPIA for the TAD. However, we found that PPIA increased the relative rate of isomerization at room temperature by ~300-fold (Figure 5A).

We subsequently purified and assayed each of the predominantly nuclear cyclophilins PPIE, PPIG, PPIH, PPIL1, PPIL2, PPIL3, PPWD, and CWC27 for activity against the TAD switch by acquiring ^{15}N-^{1}H ZZ-exchange data under similar conditions at room temperature. We found that the cyclophilins PPIE, PPIG, PPIH, PPIL1, and PPIL3 all significantly increased the rate of isomerization in BMAL1, although their acceleration of exchange rates in the TAD varied by over 10-fold (Figures 5A and 5B). By contrast, the isomerases PPIL2, PPWD, and CWC27 either were not active on the TAD or had activity that was below the detection limit of our ^{15}N-^{1}H ZZ-exchange assay. Both PPIL2 and CWC27 were previously shown to lack activity on generic peptide substrates used to assay cyclophilin activity, suggesting that they are catalytically dead (Davis et al., 2010). We then explored whether cyclophilin activity on the TAD was restricted

Table 2. Kinetics of *cis/trans* Isomerization at the TAD Switch as Measured by ^{15}N-^{1}H ZZ-Exchange NMR Spectroscopy

	Rate of Isomerization, s^{-1}		Time per Isomerization Event, s	
Temperature, °C	*cis* → *trans*	*trans* → *cis*	*cis* → *trans*	*trans* → *cis*
25[a]	4.58×10^{-3}	2.64×10^{-3}	218.34	378.78
37[a]	2.33×10^{-2}	1.35×10^{-2}	42.92	74.07
55	2.15×10^{-1}	1.24×10^{-1}	4.65	8.06
60	3.82×10^{-1}	2.20×10^{-1}	2.62	4.55
65	6.67×10^{-1}	3.84×10^{-1}	1.50	2.60

[a]Values were extrapolated from an Eyring plot.

to isoforms with nuclear localization by testing the activity of PPIF (also known as CypD), which is localized exclusively in mitochondria (Lin and Lechleiter, 2002). We found that PPIF was at least as active on the TAD as the top-ranked nuclear cyclophilins in our assay (Figures 5A and 5B), indicating that cyclophilins can exhibit robust activity on the BMAL1 TAD when removed from a cellular context that might otherwise impart substrate selectivity. To date, very little is known about factors that dictate the substrate selectivity or activity of cyclophilins, although they share relatively similar active sites (Davis et al., 2010). Notably, some of the cyclophilins that are active on the BMAL1 TAD in vitro are also expressed in a circadian manner in vivo (Figure S5; Pizarro et al., 2013). Therefore, the selectivity and/or activity of cyclophilins on the TAD may be conferred in vivo by regulated changes in abundance, subcellular localization, or through formation of different regulatory complexes with CLOCK:BMAL1 throughout the day (Koike et al., 2012; Lee et al., 2001).

Inhibition of Cyclophilins Increases Circadian Period Length

To explore whether cyclophilins influence timekeeping by the mammalian circadian clock, we treated human U2OS osteosarcoma cells stably transfected with a *Bmal1-dLuc* bioluminescent circadian reporter (Vollmers et al., 2008) with the broad specificity cyclophilin inhibitor, cyclosporin A (CsA). This cell-permeable cyclic peptide binds to the active site of the cyclophilin family with affinities ranging from ~5 to ~500 nM (Davis et al., 2010). We observed dose-dependent lengthening of the circadian period with low doses of CsA (Figures 5C and 5D), whereas at high concentrations (>15 μM), it induced arrhythmicity (data not shown). To probe the selectivity of CsA on cyclophilin regulation of the BMAL1 TAD, we performed two additional orthogonal assays. First, we examined whether the long-period phenotype could be attributed to inhibition of the phosphatase PP2B, as CsA can also direct the assembly of inhibitory ternary complexes of cyclophilins with PP2B (Huai et al., 2002; Liu et al., 1991). The effect of CsA on the circadian period appeared to be independent of PP2B, as we found that treatment with deltamethrin, a cyclophilin-independent PP2B inhibitor (Enan and Matsumura, 1992), did not elicit a change in period (Figures 5C and 5D). Therefore, broad inhibition of isomerase activity in the cyclophilin family leads to changes in circadian period.

We then wanted to determine the degree to which CsA-dependent changes in period arose from regulation of the BMAL1 TAD switch. To do this, we utilized stable *Bmal1*$^{-/-}$;*Per2*^{Luc} cell lines complemented with either WT *Bmal1* or two *trans*-locked *Bmal1* mutants, P625A or W624A/P625A (Figures 2 and S5). We reasoned that any CsA-dependent period changes in the mutant lines could not be due to regulation of the switch by cyclophilins, as the *cis* isomer of the switch was eliminated upon introduction of these mutations (Figures 2 and S2). Consistent with this model, we observed a significant decrease in period lengthening by CsA in both *trans*-locked cell lines, compared to cells complemented with WT *Bmal1* (Figures 5E and S5). Switch-independent changes in period, particularly at the highest concentration of CsA tested (10 μM), demonstrate that regulation of other pathways aside from the TAD switch by cyclophilins can also influence circadian timing. Taken together, our data support a role for an intrinsically slow conformational switch in the BMAL1 TAD in regulation of the circadian period and lay the foundation for studies of clock regulation by cyclophilins, a broadly expressed, yet poorly studied, class of enzymes.

DISCUSSION

Here, we present our discovery of a slow conformational switch in the BMAL1 TAD that participates in the regulation of timekeeping by the mammalian circadian clock. Using NMR spectroscopy, we identified that *cis/trans* isomerization about the W624-P625 imide bond at the C terminus of BMAL1 underlies the molecular basis for this binary switch. Consistent with previous studies on the composition and rarity of other switches based on *cis/trans* isomerization (Shen and Bax, 2010; Stewart et al., 1990), we found that both proline and tryptophan side chains make critical contributions to the relatively high *cis* population observed in the BMAL1 TAD. These two residues are conserved from humans to invertebrates (including insects other than *Drosophila*) that have a vertebrate-like clock architecture (Chang et al., 2003), suggesting an ancient role for the TAD switch in the regulation of CLOCK:BMAL1 activity. We used mutation of the Trp and Pro sites to generate a suite of TAD proteins with varying *cis/trans* populations or mutants that were altogether "locked" into discrete *cis* or *trans* isomers. By coupling cell-based studies of circadian oscillations with solution biophysical techniques that probed structural and biochemical constraints of the TAD switch, we were able to demonstrate that perturbing switch function alters circadian timing. Moreover, we identified that cyclophilins can accelerate interconversion in vitro and influence circadian timing in clock cells in a switch-dependent manner, suggesting that cyclophilins regulate the clock, at least partly, through control of the TAD switch.

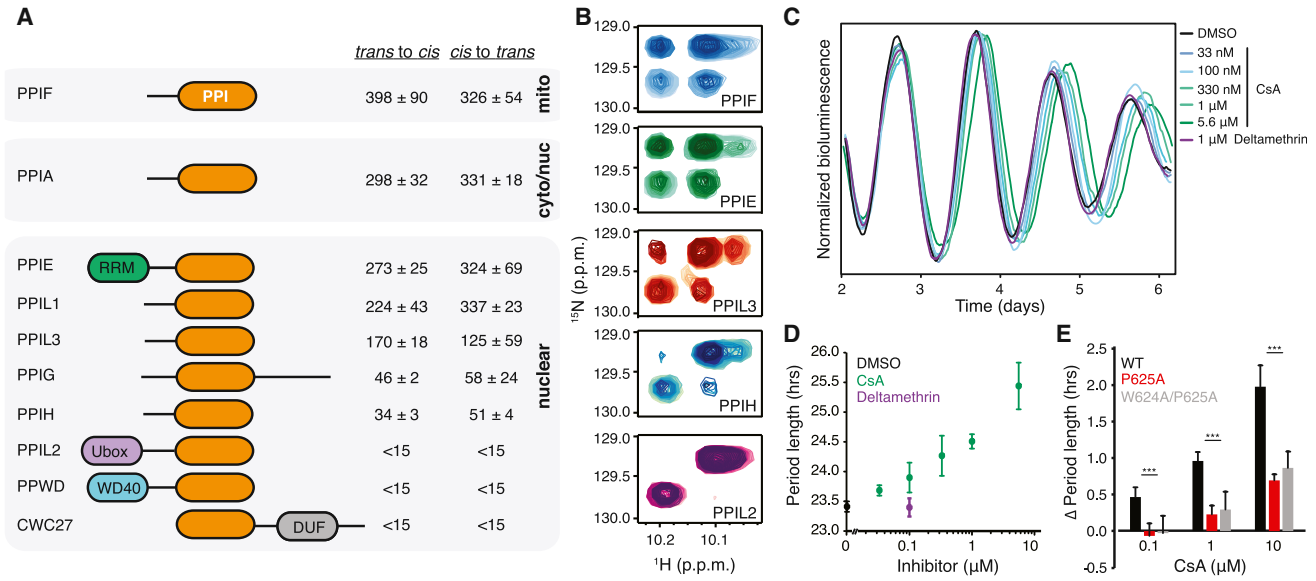

Figure 5. Cyclophilins Accelerate Isomerization of the TAD Switch to Regulate Circadian Period

(A) Domain schematics for cyclophilins tested against the BMAL1 TAD and relative rate enhancement compared to uncatalyzed isomerization at room temperature. cyto/nuc, cytoplasmic/nuclear; mito, mitochondrial.

(B) Highlighted region of ^{15}N-^{1}H ZZ-exchange spectra displaying the W624 indole of the ^{15}N TAD with indicated cyclophilins. Spectra from a ZZ-exchange time delay series (delay = 0–1 s) are overlaid in sequentially darker colors.

(C) Synchronized circadian bioluminescence records from U2OS *Bmal1-dLuc* fibroblasts in the presence of DMSO, CsA, or deltamethrin. One individual trace shown for clarity from two independent assays with n = 3 replicates.

(D) Mean circadian period of cultures upon treatment with DMSO (black), CsA (green), or deltamethrin (purple) ± SD from n = 3 replicates with two independent assays.

(E) Comparison of mean period changes ± SD as a function of CsA concentration in *Bmal1*$^{-/-}$;*Per2*^{Luc} fibroblasts complemented with WT (black), P625A (red), or W624A/P625A (gray) *Bmal1*. ***p < 0.01, compared to WT *Bmal1* by two-tailed t test.

See also Figure S5.

There is growing evidence that the flexible BMAL1 TAD plays an important role in the control of circadian timekeeping. Given that transcription-based feedback loops establish the mammalian circadian clock, factors that influence how the CLOCK:BMAL1 interacts with regulators are likely to play a key role in timekeeping (Gustafson and Partch, 2015). The conformational switch that we identified by NMR is located in the C terminus of an intrinsically disordered transactivation domain that is essential for CLOCK:BMAL1 activity and circadian timekeeping (Park et al., 2015; Xu et al., 2015). Notably, the importance of this switch region was first highlighted a decade ago in a transposon-based screen to identify functionally important regions of BMAL1; Yagita and colleagues noted that truncation of the last seven amino acids of BMAL1 decreased CLOCK:BMAL1 activity and impaired cycling (Kiyohara et al., 2006). We recently showed that this same region makes a significant contribution to binding both positive and negative transcriptional regulators by cooperating with a conserved alpha helical element in the TAD to influence clock timing (Xu et al., 2015). The data presented here identify yet another example of how the flexible BMAL1 TAD influences circadian timing and demonstrate the functional importance of protein dynamics at the TAD over an apparent 12 orders of magnitude.

Proline isomerization has demonstrated roles at each step of transcriptional regulation, from protein folding and regulation of transcription factor interactions to modification and recognition of histone tails, and conformational control of the RNA polymerase II (Pol II) C-terminal domain that controls its activity (reviewed in Hanes, 2015). Although we provide evidence in support of a binary conformational switch in the TAD by NMR and its ability to influence circadian timekeeping in cellular reconstitution assays, we still don't understand exactly how the switch regulates circadian period. Timekeeping by the circadian clock depends on the regulated transition through a series of transcriptional regulatory complexes on DNA throughout the day (Koike et al., 2012). This dynamic conformational switch could hinder the formation of highly stable complexes to play a role in the recognition and handoff between transcriptional coactivators and repressors at CLOCK:BMAL1. Other transcription factors such as p53, c-Myb, and CREB utilize conformational changes at their TADs to control their activation state. While this most commonly arises from binding-induced changes in structure (Borcherds et al., 2014; Parker et al., 1999; Sugase et al., 2007), there is also evidence that slow events controlled by proline isomerization can play an important role in some cases (Follis et al., 2015). Our data demonstrate that both W624 and P625 establish the switch and contribute to normal circadian timekeeping. Interestingly, the W624A mutation not only locks the switch into its *trans* isomer but also leads to an additional shortening of the period that is strikingly similar to the phenotype observed upon deletion

of the entire switch region (Xu et al., 2015). Therefore, we believe that identifying the structural role that W624 plays in assembling complexes with transcriptional regulators will likely help identify how the TAD switch regulates CLOCK:BMAL1 activity.

To date, conformational control by proline isomerization has been relatively poorly studied, due to the difficulty in identification and analysis of the process in vitro and in the cellular milieu. Similarly, our understanding of the PPIases that regulate this intrinsically slow process in the cellular context has lagged behind that of other signaling enzymes such as kinases and phosphatases. We have a solid understanding how kinases, phosphatases, and other enzymes that control chemical modification of clock proteins exert powerful roles in modulating clock timing (Gallego and Virshup, 2007). We provide evidence here that isomerases of the cyclophilin family accelerate the intrinsically slow *cis/trans* isomerization of the BMAL1 TAD by up to several 100-fold in vitro. Moreover, studies with the broad specificity inhibitor CsA suggest that cyclophilins contribute to circadian timekeeping in cells in a TAD switch-dependent manner. Interestingly, we found that a number of cyclophilins that are active on the BMAL1 TAD are also expressed in vivo on a circadian timescale, suggesting the possibility for modes of feedback regulation that are common in circadian rhythms (Baggs et al., 2009). These findings are strengthened by the observation that animals with chronic administration of PPIase inhibitors exhibit defects in circadian cycling (Katz et al., 2008), as do organ transplant patients on long-term dosing of CsA (Kooman et al., 2001; van de Borne et al., 1993; van den Dorpel et al., 1996). More work is needed to parse out the potentially redundant roles of cyclophilins and, possibly, other proline isomerases on the BMAL1 TAD. However, our findings are consistent with two studies showing that the isomerase PPIE (also known as Cyp33) binds to the histone methyltransferase MLL1 to modulate its activity (Wang et al., 2010), which is, in turn, recruited to the CLOCK:BMAL1 complex in a circadian-dependent manner (Katada and Sassone-Corsi, 2010). Conceivably, MLL1-bound PPIE may also promote prolyl isomerization within the BMAL1 TAD when assembled within a CLOCK:BMAL1:MLL1 complex, lending credence to a model in which these ubiquitous enzymes may be recruited to and act upon the molecular timer in a circadian fashion.

STAR★METHODS

Detailed methods are provided in the online version of this paper and include the following:

- KEY RESOURCES TABLE
- CONTACT FOR REAGENTS AND RESOURCE SHARING
- EXPERIMENTAL MODEL AND SUBJECT DETAILS
  - Cell lines
- METHOD DETAILS
  - Lentiviral DNA constructs, transduction, and analysis
  - Bioluminescence recording and data analysis
  - Expression and purification of recombinant proteins
  - Peptide synthesis and purification
  - Mass spectrometry
  - NMR spectroscopy
  - Fluorescence anisotropy
  - Isothermal titration calorimetry
- QUANTIFICATION AND STATISTICAL ANALYSIS
  - Cellular Period Analysis
  - Analysis of *cis*/trans isomerization rates
- DATA AND SOFTWARE AVAILABILITY

SUPPLEMENTAL INFORMATION

Supplemental Information includes five figures and can be found with this article online at http://dx.doi.org/10.1016/j.molcel.2017.04.011.

AUTHOR CONTRIBUTIONS

C.L.G., N.C.P., H.A., H.-W.L., and C.L.P. designed the experiments. C.L.G., N.C.P., H.A., C.A., A.K.M., and C.L.P. collected data. H.X., O.L.W., and T.L.D. contributed reagents or analytical tools. A.C.L. and C.L.P. supervised the experiments. C.L.G. and C.L.P. wrote the manuscript, with contributions from T.L.D. and A.C.L. All authors reviewed the manuscript and approved of the conclusions.

ACKNOWLEDGMENTS

We thank John Hogenesch (University of Cincinnati) for the U2OS *Bmal1-dLuc* cell line and Peter Wright (The Scripps Research Institute) for a plasmid encoding the KIX domain of mouse CBP. Thanks to Joshua Schwochert, Cameron Pye, and Scott Lokey for training and providing resources for custom peptide synthesis. We thank Walter Bray in the UCSC Chemical Screening Center and Qiangli Zhang in the UCSC Mass Spectrometry Facility for access to instrumentation. Funding for the UCSC Mass Spectrometry Facility was provided by the W.M. Keck Foundation (grant 001768) and the NIH National Center for Research Resources (grant S10RR020939). This work was supported by NIH grants R01 GM107069 (to C.L.P.) and R00 GM094293 (to T.L.D.) and by NSF grant IOS-0920417 (to A.C.L.). A.K.M. was supported by NIH Ruth Kirschstein predoctoral fellowship F31 CA189660.

Received: December 14, 2016
Revised: March 18, 2017
Accepted: April 13, 2017
Published: May 11, 2017

SUPPORTING CITATIONS

The following references appear in the Supplemental Information: Hughes et al. (2009); Hughes et al. (2010).

REFERENCES

Adams, B.M., Coates, M.N., Jackson, S.R., Jurica, M.S., and Davis, T.L. (2015). Nuclear cyclophilins affect spliceosome assembly and function in vitro. Biochem. J. *469*, 223–233.

Baggs, J.E., Price, T.S., DiTacchio, L., Panda, S., Fitzgerald, G.A., and Hogenesch, J.B. (2009). Network features of the mammalian circadian clock. PLoS Biol. *7*, e52.

Bataille, A.R., Jeronimo, C., Jacques, P.E., Laramée, L., Fortin, M.E., Forest, A., Bergeron, M., Hanes, S.D., and Robert, F. (2012). A universal RNA polymerase II CTD cycle is orchestrated by complex interplays between kinase, phosphatase, and isomerase enzymes along genes. Mol. Cell *45*, 158–170.

Borcherds, W., Theillet, F.X., Katzer, A., Finzel, A., Mishall, K.M., Powell, A.T., Wu, H., Manieri, W., Dieterich, C., Selenko, P., et al. (2014). Disorder and residual helicity alter p53-Mdm2 binding affinity and signaling in cells. Nat. Chem. Biol. *10*, 1000–1002.

Brazin, K.N., Mallis, R.J., Fulton, D.B., and Andreotti, A.H. (2002). Regulation of the tyrosine kinase Itk by the peptidyl-prolyl isomerase cyclophilin A. Proc. Natl. Acad. Sci. USA *99*, 1899–1904.

Chang, D.C., McWatters, H.G., Williams, J.A., Gotter, A.L., Levine, J.D., and Reppert, S.M. (2003). Constructing a feedback loop with circadian clock molecules from the silkmoth, *Antheraea pernyi*. J. Biol. Chem. *278*, 38149–38158.

Coelmont, L., Hanoulle, X., Chatterji, U., Berger, C., Snoeck, J., Bobardt, M., Lim, P., Vliegen, I., Paeshuyse, J., Vuagniaux, G., et al. (2010). DEB025 (Alisporivir) inhibits hepatitis C virus replication by preventing a cyclophilin A induced cis-trans isomerisation in domain II of NS5A. PLoS ONE *5*, e13687.

Czarna, A., Berndt, A., Singh, H.R., Grudziecki, A., Ladurner, A.G., Timinszky, G., Kramer, A., and Wolf, E. (2013). Structures of *Drosophila* cryptochrome and mouse cryptochrome1 provide insight into circadian function. Cell *153*, 1394–1405.

Davis, T.L., Walker, J.R., Campagna-Slater, V., Finerty, P.J., Paramanathan, R., Bernstein, G., MacKenzie, F., Tempel, W., Ouyang, H., Lee, W.H., et al. (2010). Structural and biochemical characterization of the human cyclophilin family of peptidyl-prolyl isomerases. PLoS Biol. *8*, e1000439.

Delaglio, F., Grzesiek, S., Vuister, G.W., Zhu, G., Pfeifer, J., and Bax, A. (1995). NMRPipe: a multidimensional spectral processing system based on UNIX pipes. J. Biomol. NMR *6*, 277–293.

Eckert, B., Martin, A., Balbach, J., and Schmid, F.X. (2005). Prolyl isomerization as a molecular timer in phage infection. Nat. Struct. Mol. Biol. *12*, 619–623.

Enan, E., and Matsumura, F. (1992). Specific inhibition of calcineurin by type II synthetic pyrethroid insecticides. Biochem. Pharmacol. *43*, 1777–1784.

Farrow, N.A., Zhang, O., Forman-Kay, J.D., and Kay, L.E. (1994). A heteronuclear correlation experiment for simultaneous determination of 15N longitudinal decay and chemical exchange rates of systems in slow equilibrium. J. Biomol. NMR *4*, 727–734.

Ferrell, J.E., Jr., and Cimprich, K.A. (2003). Enforced proximity in the function of a famous scaffold. Mol. Cell *11*, 289–291.

Follis, A.V., Llambi, F., Merritt, P., Chipuk, J.E., Green, D.R., and Kriwacki, R.W. (2015). Pin1-induced proline isomerization in cytosolic p53 mediates BAX activation and apoptosis. Mol. Cell *59*, 677–684.

Gallego, M., and Virshup, D.M. (2007). Post-translational modifications regulate the ticking of the circadian clock. Nat. Rev. Mol. Cell Biol. *8*, 139–148.

Grathwohl, C., and Wüthrich, K. (1981). NMR studies of the rates of proline *cis-trans* isomerization in oligopeptides. Biopolymers *20*, 2623–2633.

Gustafson, C.L., and Partch, C.L. (2015). Emerging models for the molecular basis of mammalian circadian timing. Biochemistry *54*, 134–149.

Hanes, S.D. (2015). Prolyl isomerases in gene transcription. Biochim. Biophys. Acta *1850*, 2017–2034.

Henzler-Wildman, K., and Kern, D. (2007). Dynamic personalities of proteins. Nature *450*, 964–972.

Huai, Q., Kim, H.Y., Liu, Y., Zhao, Y., Mondragon, A., Liu, J.O., and Ke, H. (2002). Crystal structure of calcineurin-cyclophilin-cyclosporin shows common but distinct recognition of immunophilin-drug complexes. Proc. Natl. Acad. Sci. USA *99*, 12037–12042.

Hughes, M.E., DiTacchio, L., Hayes, K.R., Vollmers, C., Pulivarthy, S., Baggs, J.E., Panda, S., and Hogenesch, J.B. (2009). Harmonics of circadian gene transcription in mammals. PLoS Genet. *5*, e1000442.

Hughes, M.E., Hogenesch, J.B., and Kornacker, K. (2010). JTK_CYCLE: an efficient nonparametric algorithm for detecting rhythmic components in genome-scale data sets. J. Biol. Rhythms *25*, 372–380.

Johnson, B.A. (2004). Using NMRView to visualize and analyze the NMR spectra of macromolecules. Methods Mol. Biol. *278*, 313–352.

Kang, S.W., Lee, E., Cho, E., Seo, J.H., Ko, H.W., and Kim, E.Y. (2015). Drosophila peptidyl-prolyl isomerase Pin1 modulates circadian rhythms via regulating levels of PERIOD. Biochem. Biophys. Res. Commun. *463*, 235–240.

Katada, S., and Sassone-Corsi, P. (2010). The histone methyltransferase MLL1 permits the oscillation of circadian gene expression. Nat. Struct. Mol. Biol. *17*, 1414–1421.

Katz, M.E., Simonetta, S.H., Ralph, M.R., and Golombek, D.A. (2008). Immunosuppressant calcineurin inhibitors phase shift circadian rhythms and inhibit circadian responses to light. Pharmacol. Biochem. Behav. *90*, 763–768.

Kiyohara, Y.B., Tagao, S., Tamanini, F., Morita, A., Sugisawa, Y., Yasuda, M., Yamanaka, I., Ueda, H.R., van der Horst, G.T., Kondo, T., and Yagita, K. (2006). The BMAL1 C terminus regulates the circadian transcription feedback loop. Proc. Natl. Acad. Sci. USA *103*, 10074–10079.

Kleckner, I.R., and Foster, M.P. (2011). An introduction to NMR-based approaches for measuring protein dynamics. Biochim. Biophys. Acta *1814*, 942–968.

Koike, N., Yoo, S.H., Huang, H.C., Kumar, V., Lee, C., Kim, T.K., and Takahashi, J.S. (2012). Transcriptional architecture and chromatin landscape of the core circadian clock in mammals. Science *338*, 349–354.

Kooman, J.P., Christiaans, M.H., Boots, J.M., van Der Sande, F.M., Leunissen, K.M., and van Hooff, J.P. (2001). A comparison between office and ambulatory blood pressure measurements in renal transplant patients with chronic transplant nephropathy. Am. J. Kidney Dis. *37*, 1170–1176.

Lang, K., Schmid, F.X., and Fischer, G. (1987). Catalysis of protein folding by prolyl isomerase. Nature *329*, 268–270.

Lee, C., Etchegaray, J.P., Cagampang, F.R., Loudon, A.S., and Reppert, S.M. (2001). Posttranslational mechanisms regulate the mammalian circadian clock. Cell *107*, 855–867.

Lin, D.T., and Lechleiter, J.D. (2002). Mitochondrial targeted cyclophilin D protects cells from cell death by peptidyl prolyl isomerization. J. Biol. Chem. *277*, 31134–31141.

Liou, Y.C., Zhou, X.Z., and Lu, K.P. (2011). Prolyl isomerase Pin1 as a molecular switch to determine the fate of phosphoproteins. Trends Biochem. Sci. *36*, 501–514.

Lipton, J.O., Yuan, E.D., Boyle, L.M., Ebrahimi-Fakhari, D., Kwiatkowski, E., Nathan, A., Güttler, T., Davis, F., Asara, J.M., and Sahin, M. (2015). The circadian protein BMAL1 regulates translation in response to S6K1-mediated phosphorylation. Cell *161*, 1138–1151.

Liu, H., and Naismith, J.H. (2008). An efficient one-step site-directed deletion, insertion, single and multiple-site plasmid mutagenesis protocol. BMC Biotechnol. *8*, 91.

Liu, J., Farmer, J.D., Jr., Lane, W.S., Friedman, J., Weissman, I., and Schreiber, S.L. (1991). Calcineurin is a common target of cyclophilin-cyclosporin A and FKBP-FK506 complexes. Cell *66*, 807–815.

Liu, A.C., Tran, H.G., Zhang, E.E., Priest, A.A., Welsh, D.K., and Kay, S.A. (2008). Redundant function of REV-ERBalpha and beta and non-essential role for Bmal1 cycling in transcriptional regulation of intracellular circadian rhythms. PLoS Genet. *4*, e1000023.

Lu, K.P., Finn, G., Lee, T.H., and Nicholson, L.K. (2007). Prolyl *cis-trans* isomerization as a molecular timer. Nat. Chem. Biol. *3*, 619–629.

Lummis, S.C., Beene, D.L., Lee, L.W., Lester, H.A., Broadhurst, R.W., and Dougherty, D.A. (2005). *Cis-trans* isomerization at a proline opens the pore of a neurotransmitter-gated ion channel. Nature *438*, 248–252.

Nakamura, K., Greenwood, A., Binder, L., Bigio, E.H., Denial, S., Nicholson, L., Zhou, X.Z., and Lu, K.P. (2012). Proline isomer-specific antibodies reveal the early pathogenic tau conformation in Alzheimer's disease. Cell *149*, 232–244.

Nelson, C.J., Santos-Rosa, H., and Kouzarides, T. (2006). Proline isomerization of histone H3 regulates lysine methylation and gene expression. Cell *126*, 905–916.

Pal, D., and Chakrabarti, P. (1999). *Cis* peptide bonds in proteins: residues involved, their conformations, interactions and locations. J. Mol. Biol. *294*, 271–288.

Palmer, A.G., 3rd, Kroenke, C.D., and Loria, J.P. (2001). Nuclear magnetic resonance methods for quantifying microsecond-to-millisecond motions in biological macromolecules. Methods Enzymol. *339*, 204–238.

Park, N., Kim, H.D., Cheon, S., Row, H., Lee, J., Han, D.H., Cho, S., and Kim, K. (2015). A novel Bmal1 mutant mouse reveals essential roles of the C-terminal domain on circadian rhythms. PLoS ONE *10*, e0138661.

Parker, D., Rivera, M., Zor, T., Henrion-Caude, A., Radhakrishnan, I., Kumar, A., Shapiro, L.H., Wright, P.E., Montminy, M., and Brindle, P.K. (1999). Role of secondary structure in discrimination between constitutive and inducible activators. Mol. Cell. Biol. *19*, 5601–5607.

Partch, C.L., Green, C.B., and Takahashi, J.S. (2014). Molecular architecture of the mammalian circadian clock. Trends Cell Biol. *24*, 90–99.

Peterson, K.J., Lyons, J.B., Nowak, K.S., Takacs, C.M., Wargo, M.J., and McPeek, M.A. (2004). Estimating metazoan divergence times with a molecular clock. Proc. Natl. Acad. Sci. USA *101*, 6536–6541.

Phillips, A.H., Zhang, Y., Cunningham, C.N., Zhou, L., Forrest, W.F., Liu, P.S., Steffek, M., Lee, J., Tam, C., Helgason, E., et al. (2013). Conformational dynamics control ubiquitin-deubiquitinase interactions and influence in vivo signaling. Proc. Natl. Acad. Sci. USA *110*, 11379–11384.

Pizarro, A., Hayer, K., Lahens, N.F., and Hogenesch, J.B. (2013). CircaDB: a database of mammalian circadian gene expression profiles. Nucleic Acids Res. *41*, D1009–D1013.

Pullen, L., and Bolon, D.N. (2011). Enforced N-domain proximity stimulates Hsp90 ATPase activity and is compatible with function in vivo. J. Biol. Chem. *286*, 11091–11098.

Ramanathan, C., Khan, S.K., Kathale, N.D., Xu, H., and Liu, A.C. (2012). Monitoring cell-autonomous circadian clock rhythms of gene expression using luciferase bioluminescence reporters. J. Vis. Exp. (67), 4234.

Reimer, U., Scherer, G., Drewello, M., Kruber, S., Schutkowski, M., and Fischer, G. (1998). Side-chain effects on peptidyl-prolyl *cis/trans* isomerisation. J. Mol. Biol. *279*, 449–460.

Rubin, E.B., Shemesh, Y., Cohen, M., Elgavish, S., Robertson, H.M., and Bloch, G. (2006). Molecular and phylogenetic analyses reveal mammalian-like clockwork in the honey bee (*Apis mellifera*) and shed new light on the molecular evolution of the circadian clock. Genome Res. *16*, 1352–1365.

Saleh, T., Jankowski, W., Sriram, G., Rossi, P., Shah, S., Lee, K.B., Cruz, L.A., Rodriguez, A.J., Birge, R.B., and Kalodimos, C.G. (2016). Cyclophilin A promotes cell migration via the Abl-Crk signaling pathway. Nat. Chem. Biol. *12*, 117–123.

Sarkar, P., Reichman, C., Saleh, T., Birge, R.B., and Kalodimos, C.G. (2007). Proline *cis-trans* isomerization controls autoinhibition of a signaling protein. Mol. Cell *25*, 413–426.

Schmid, F.X. (1993). Prolyl isomerase: enzymatic catalysis of slow protein-folding reactions. Annu. Rev. Biophys. Biomol. Struct. *22*, 123–142.

Sheffield, P., Garrard, S., and Derewenda, Z. (1999). Overcoming expression and purification problems of RhoGDI using a family of "parallel" expression vectors. Protein Expr. Purif. *15*, 34–39.

Shen, Y., and Bax, A. (2010). Prediction of Xaa-Pro peptide bond conformation from sequence and chemical shifts. J. Biomol. NMR *46*, 199–204.

Shi, S., Hida, A., McGuinness, O.P., Wasserman, D.H., Yamazaki, S., and Johnson, C.H. (2010). Circadian clock gene Bmal1 is not essential; functional replacement with its paralog, Bmal2. Curr. Biol. *20*, 316–321.

Stewart, D.E., Sarkar, A., and Wampler, J.E. (1990). Occurrence and role of *cis* peptide bonds in protein structures. J. Mol. Biol. *214*, 253–260.

Sugase, K., Dyson, H.J., and Wright, P.E. (2007). Mechanism of coupled folding and binding of an intrinsically disordered protein. Nature *447*, 1021–1025.

Theillet, F.X., Binolfi, A., Frembgen-Kesner, T., Hingorani, K., Sarkar, M., Kyne, C., Li, C., Crowley, P.B., Gierasch, L., Pielak, G.J., et al. (2014). Physicochemical properties of cells and their effects on intrinsically disordered proteins (IDPs). Chem. Rev. *114*, 6661–6714.

van de Borne, P., Gelin, M., Van de Stadt, J., and Degaute, J.P. (1993). Circadian rhythms of blood pressure after liver transplantation. Hypertension *21*, 398–405.

van den Dorpel, M.A., van den Meiracker, A.H., Lameris, T.W., Boomsma, F., Levi, M., Man in 't Veld, A.J., Weimar, W., and Schalekamp, M.A. (1996). Cyclosporin A impairs the nocturnal blood pressure fall in renal transplant recipients. Hypertension *28*, 304–307.

Vollmers, C., Panda, S., and DiTacchio, L. (2008). A high-throughput assay for siRNA-based circadian screens in human U2OS cells. PLoS ONE *3*, e3457.

Wang, Z., Song, J., Milne, T.A., Wang, G.G., Li, H., Allis, C.D., and Patel, D.J. (2010). Pro isomerization in MLL1 PHD3-bromo cassette connects H3K4me readout to CyP33 and HDAC-mediated repression. Cell *141*, 1183–1194.

Wedemeyer, W.J., Welker, E., and Scheraga, H.A. (2002). Proline cis-trans isomerization and protein folding. Biochemistry *41*, 14637–14644.

Xu, H., Gustafson, C.L., Sammons, P.J., Khan, S.K., Parsley, N.C., Ramanathan, C., Lee, H.W., Liu, A.C., and Partch, C.L. (2015). Cryptochrome 1 regulates the circadian clock through dynamic interactions with the BMAL1 C terminus. Nat. Struct. Mol. Biol. *22*, 476–484.

Zhang, Z., and Marshall, A.G. (1998). A universal algorithm for fast and automated charge state deconvolution of electrospray mass-to-charge ratio spectra. J. Am. Soc. Mass Spectrom. *9*, 225–233.

Zhang, R., Lahens, N.F., Ballance, H.I., Hughes, M.E., and Hogenesch, J.B. (2014). A circadian gene expression atlas in mammals: implications for biology and medicine. Proc. Natl. Acad. Sci. USA *111*, 16219–16224.

Zhou, X.Z., and Lu, K.P. (2016). The isomerase PIN1 controls numerous cancer-driving pathways and is a unique drug target. Nat. Rev. Cancer *16*, 463–478.

Zhu, H., Sauman, I., Yuan, Q., Casselman, A., Emery-Le, M., Emery, P., and Reppert, S.M. (2008). Cryptochromes define a novel circadian clock mechanism in monarch butterflies that may underlie sun compass navigation. PLoS Biol. *6*, e4.

Zondlo, N.J. (2013). Aromatic-proline interactions: electronically tunable CH/π interactions. Acc. Chem. Res. *46*, 1039–1049.

STAR★METHODS

KEY RESOURCES TABLE

REAGENT or RESOURCE	SOURCE	IDENTIFIER
Antibodies		
Mouse monoclonal anti-Flag (M2)	Sigma	Cat# F3165; RRID: AB_259529
Goat polyclonal anti-beta actin (C-11)	Santa Cruz Biotechnology	Cat# sc-1615; RRID: AB_630835
Bacterial and Virus Strains		
DH5α	Invitrogen	Cat# 18265017
Rosetta (DE3)	EMD Millipore	Cat# 70954
Chemicals, Peptides, and Recombinant Proteins		
Dexamethasone	Sigma	Cat# D4902
D-Luciferin Firefly, Potassium salt	Research Products International	Cat# L37060
B-27 vitamin supplement	Thermo Fisher	Cat# 17504044
Cyclosporin A	Sigma	Cat# 30024
Deltamethrin	Sigma	Cat# D9315
^{15}N ammonium chloride (^{15}N, 99%)	Cambridge Isotope Laboratories	Cat# NLM-467
Fmoc-5,5 dimethyl Proline	PolyPeptide Group	Cat# FA21702
mBMAL1 peptide: DFSDLPWPL	This study	N/A
mBMAL1 peptide: FSDLPWPL	This study	N/A
mBMAL1 peptide: FSDLPAPL	This study	N/A
mBMAL1 peptide: FSDLPWAL	This study	N/A
mBMAL1 peptide: FSDLPWdmPL	This study	N/A
mBMAL1 peptide: FSDLPFPL	Bio-Synthesis	N/A
mBMAL1 peptide: FSDLPYPL	Bio-Synthesis	N/A
iBMAL1 peptide: FSGLPWPLP	Bio-Synthesis	N/A
mBMAL1 peptide: short TAD P625dmP	Bio-Synthesis	N/A
mBMAL1 peptide: short TAD with N-terminal 5,6-TAMRA	Bio-Synthesis	N/A
mBMAL1 peptide: short TAD P625A with N-terminal 5,6-TAMRA	Bio-Synthesis	N/A
mBMAL1 peptide: short TAD P625dmP with N-terminal 5,6-TAMRA	Bio-Synthesis	N/A
mBMAL1 peptide: short TAD Δswitch with N-terminal 5,6-TAMRA	Bio-Synthesis	N/A
mCRY1 CC helix peptide	Xu et al., 2015	N/A
mBmal1 TAD	This study	N/A
mBmal1 short TAD	This study	N/A
mBmal1 TAD W624A	This study	N/A
mBmal1 TAD P625A	This study	N/A
mBmal1 TAD Δswitch	This study	N/A
mCBP KIX	Xu et al., 2015	N/A
mCRY1 PHR	This study	N/A
His-PPIA	This study	N/A
His-PPIE	This study	N/A
His-PPIF	This study	N/A
His-PPIG (isomerase domain)	This study	N/A
His-PPIH	This study	N/A
His-PPIL1	This study	N/A

(*Continued on next page*)

Continued

REAGENT or RESOURCE	SOURCE	IDENTIFIER
His-PPIL2	This study	N/A
HisGST-PPIL3	This study	N/A
His-PPWD (isomerase domain)	This study	N/A
His-CWC27 (isomerase domain)	This study	N/A
His-TEV Δ238	This study	N/A
Deposited Data		
Source western blot images for Figure S2	This study; Mendeley Data	http://dx.doi.org/10.17632/35zchh9fsb.1
^{15}N-^{1}H ZZ exchange NMR time series data at 25°C	This study; Mendeley Data	http://dx.doi.org/10.17632/4hs472w6wb.1
^{15}N-^{1}H ZZ exchange NMR time series data at 55°C	This study; Mendeley Data	http://dx.doi.org/10.17632/8yx9wzt9gh.1
^{15}N-^{1}H ZZ exchange NMR time series data at 60°C	This study; Mendeley Data	http://dx.doi.org/10.17632/gjfjvjpvdr.1
^{15}N-^{1}H ZZ exchange NMR time series data at 65°C	This study; Mendeley Data	http://dx.doi.org/10.17632/kn58vc7hww.1
^{15}N-^{1}H ZZ exchange NMR time series data with PPIA	This study; Mendeley Data	http://dx.doi.org/10.17632/4txk4b3w5g.1
^{15}N-^{1}H ZZ exchange NMR time series data with PPIE	This study; Mendeley Data	http://dx.doi.org/10.17632/pt8xjvjs2v.1
^{15}N-^{1}H ZZ exchange NMR time series data with PPIF	This study; Mendeley Data	http://dx.doi.org/10.17632/x8yn6x28x8.1
^{15}N-^{1}H ZZ exchange NMR time series data with PPIG	This study; Mendeley Data	http://dx.doi.org/10.17632/fh595ry88h.1
^{15}N-^{1}H ZZ exchange NMR time series data with PPIH	This study; Mendeley Data	http://dx.doi.org/10.17632/mpykzm4kw2.1
^{15}N-^{1}H ZZ exchange NMR time series data with PPIL1	This study; Mendeley Data	http://dx.doi.org/10.17632/f9fxfynfrb.1
^{15}N-^{1}H ZZ exchange NMR time series data with PPIL2	This study; Mendeley Data	http://dx.doi.org/10.17632/cg8fb64p5f.1
^{15}N-^{1}H ZZ exchange NMR time series data with PPIL3	This study; Mendeley Data	http://dx.doi.org/10.17632/fmhg69tcxf.1
^{15}N-^{1}H ZZ exchange NMR time series data with PPWD	This study; Mendeley Data	http://dx.doi.org/10.17632/csc3c5hs32.1
^{15}N-^{1}H ZZ exchange NMR time series data with CWC27	This study; Mendeley Data	http://dx.doi.org/10.17632/htvhkdt7rw.1
Experimental Models: Cell Lines		
Bmal1$^{-/-}$;*Per2*^{Luc} mouse embryonic fibroblasts	Liu et al., 2008	N/A
Bmal1$^{-/-}$;*Per2*^{Luc} + *Bmal1* mouse embryonic fibroblasts	Liu et al., 2008	N/A
Bmal1$^{-/-}$;*Per2*^{Luc} + *Bmal1 619X* mouse embryonic fibroblasts	Xu et al., 2015	N/A
Bmal1$^{-/-}$;*Per2*^{Luc} + *Bmal1 W624A* mouse embryonic fibroblasts	This study	N/A
Bmal1$^{-/-}$;*Per2*^{Luc} + *Bmal1 P625A* mouse embryonic fibroblasts	This study	N/A
Bmal1$^{-/-}$;*Per2*^{Luc} + *Bmal1 W624A/P625A* mouse embryonic fibroblasts	This study	N/A
U2OS *Bmal1-dLuc*	Vollmers et al., 2008	N/A
Sf9 insect cells	Expression Systems	Cat# 94-001S
Recombinant DNA		
pLV7 mBmal1	Liu et al., 2008	N/A
pLV7 mBmal1 W624A	This study	N/A
pLV7 mBmal1 P625A	This study	N/A
pLV7 mBmal1 W624A/P625A	This study	N/A
pHisGST mBmal1 TAD	This study	N/A
pHisGST mBmal1 short TAD (*E. coli* codon-optimized)	GeneWiz	N/A
pHisGST mBmal1 TAD W624A	This study	N/A
pHisGST mBmal1 TAD P625A	This study	N/A
pHisGST mBmal1 TAD Δswitch	This study	N/A
pET21 mCBP KIX	Xu et al., 2015	N/A
pFastBac mCRY1 PHR	This study	N/A
pET28 PPIA	Davis et al., 2010	N/A
pET28 PPIE	Davis et al., 2010	N/A

(*Continued on next page*)

Continued

REAGENT or RESOURCE	SOURCE	IDENTIFIER
pET28 PPIF	Davis et al., 2010	N/A
pET28 PPIG (isomerase domain)	Davis et al., 2010	N/A
pHisGST PPIH	This study	N/A
pET28 PPIL1	Davis et al., 2010	N/A
pET28 PPIL2	Davis et al., 2010	N/A
pHisGST PPIL3	This study	N/A
pET28 PPWD (isomerase domain)	Davis et al., 2010	N/A
pET28 CWC27 (isomerase domain)	Davis et al., 2010	N/A
pHis TEV Δ238	Xu et al., 2015	N/A
Software and Algorithms		
Lumicycle (version 2.54)	Actimetrics	http://actimetrics.com
Prism (version 6.0)	GraphPad Software	http://www.graphpad.com
NMRPipe/NMRDraw	Delaglio et al., 1995	http://www.ibbr.umd.edu/nmrpipe/install/html
NMRView J (version 9-2-0-b4)	One Moon Scientific	http://www.onemoonscientific.com
MATLAB (version 9.0)	MathWorks	http://www.mathworks.com
ZZ exchange NMR data analysis MATLAB script	This study; Mendeley Data	http://dx.doi.org/10.17632/w7ytgp2y9d.1

CONTACT FOR REAGENTS AND RESOURCE SHARING

Further information and requests for resources and reagents should be directed to and will be fulfilled by the Lead Contact, Carrie Partch (cpartch@ucsc.edu).

EXPERIMENTAL MODEL AND SUBJECT DETAILS

Cell lines

Isolated of the *Bmal1*$^{-/-}$;*Per2*^{Luc} line was previously described (Liu et al., 2008). The U2OS *Bmal1-dLuc* cell line was a gift from John Hogenesch (University of Cincinnati). Both cell lines were cultured in 10% DMEM (i.e., 10% (vol/vol) FBS) and 1X penicillin-streptomycin (Thermo Fisher) at 37°C in an incubator humidified with 5% CO_2. Cell lines were not authenticated.

METHOD DETAILS

Lentiviral DNA constructs, transduction, and analysis

Flag-tagged mouse *Bmal1* was cloned into pENTR/D-TOPO vector (Life Technologies) then recombined with pLV7 destination vector as previously described (Ramanathan et al., 2012). Mutations were introduced by PCR-based mutagenesis and all constructs were verified by sequencing. Production of recombinant lentiviral particles, infection and selection of *Bmal1*-complemented *Bmal1*$^{-/-}$;*Per2*^{Luc} lines was performed as described previously (Liu et al., 2008). Clonal cell lines were validated by genomic sequencing of the complemented *Bmal1* gene.

Expression of Flag-tagged *Bmal1* genes in the complemented cell lines was analyzed as before (Xu et al., 2015). Briefly, cells were lysed in RIPA buffer containing complete protease and phosphatase inhibitors (Sigma). Immunoblotting was done using the following primary antibodies: mouse anti-Flag (M2) (Sigma Cat. # F3165) and goat anti-beta actin (C-11) (Santa Cruz Biotechnology Cat. # sc-1615), and the following secondary antibodies: anti-mouse IgG-HRP (Santa Cruz Biotechnology Cat. # sc-2005) and anti-goat IgG-HRP (Santa Cruz Biotechnology Cat. # sc-2020). SuperSignal West Pico substrate (Pierce) was used for chemiluminescent detection on autoradiograph film.

Bioluminescence recording and data analysis

For real-time recording of bioluminescence, *Bmal1*$^{-/-}$;*Per2*^{Luc} and U2OS *Bmal1-dLuc* cell lines were grown to confluence in 35 mm dishes in 10% DMEM at 37°C in an incubator humidified with 5% CO_2. All cell lines were synchronized with addition of 100 nM dexamethasone in recording medium, which contained phenol red-free DMEM with 25 mM HEPES, pH 7.4, 1% (vol/vol) FBS, 1 mM luciferin and a 1X B-27 vitamin supplement (Thermo Fisher Cat. #17504044). Dishes were sealed using vacuum grease with a round 40 mm glass coverslip to minimize evaporation, and then moved to a 37°C incubator (without humidification) containing a LumiCycle

luminometer. For experiments with inhibitors, lyophilized stocks of Cyclosporin A (Sigma cat. # 30024) and Deltamethrin (Sigma cat. #D9315) were resuspended in sterile DMSO. Stocks were further diluted in DMSO such that addition of the same volume of inhibitors resulted in a final concentration of DMSO of 0.3% (vol/vol) in culture. Inhibitor stocks were pipetted into recording medium, evenly mixed, and then added to cells.

A LumiCycle luminometer (Actimetrics) was used to monitor the luminescence (counts/sec) as a function of time and data were analyzed using the LumiCycle Analysis program (version 2.54, Actimetrics). The first 24 hr of recording were omitted from data processing, and then the raw data were baseline corrected and fit to a damped sine wave, from which period length, goodness of fit, amplitude and damping rate were determined. Data were deemed acceptable if the goodness of fit exceeded 80%. For *Bmal1*$^{-/-}$;*Per2*^{Luc} cells, at least two dishes per clonal line were tested for each run with four repeats (n = 8-12). The mean trace of all recordings with standard deviation is reported.

Expression and purification of recombinant proteins

Mouse BMAL1 TAD (residues 579-626) was cloned into a bacterial expression plasmid based on the pET22b vector backbone from the parallel vector series (Sheffield et al., 1999). The BMAL1 short TAD (residues 594-626) was codon optimized for expression in *E. coli* (GeneWiz) and cloned into the same vector. All constructs possessed an N-terminal TEV cleavable His_6GST solubilizing tag and ampicillin resistance. Mutations were introduced in the TAD using a modified protocol for site-directed mutagenesis (Liu and Naismith, 2008) and confirmed with sequencing. The bacterial expression plasmid encoding the mouse CBP KIX domain (residues 585-672) was a gift from Peter Wright (The Scripps Research Institute). CBP KIX has native histidine residues that allow for the purification of the protein using Ni-NTA resin.

The Rosetta (DE3) strain of *E. coli* containing plasmids with either BMAL1 TAD or CBP KIX were grown to an OD_{600} of ~0.6-0.9 in the presence of ampicillin (100 μg/mL) and chloramphenicol (35 μg/mL). Protein expression was induced with 0.5 mM isopropyl β-D-1-thiogalactopyranoside (IPTG) and allowed to proceed for 16-18 hr at 18°C in either Luria Broth (LB) or M9 minimal medium containing 1g/L $^{15}NH_4Cl$ to generate uniformly ^{15}N-labeled proteins for NMR spectroscopy. Cells were lysed in with an Emulsiflex C-3 cell disruptor (Avestin) in Buffer A containing 50 mM Tris pH 7.5, 300 mM NaCl and 20 mM imidazole. The soluble fraction of *E. coli* lysates was passed over Ni-NTA resin (QIAGEN), washed thoroughly, and eluted using 250 mM imidazole. Fractions of interest were buffer exchanged into lysis buffer using a stirred-cell pressure concentrator with 3 kDa molecular weight cutoff filters (Amicon). Proteolysis was performed with His_6-tagged TEV protease overnight at 4°C and cleaved protein was retained from the flow-through of a Ni-NTA column. The purified protein was further purified on a preparative grade Superdex 75 16/600 size-exclusion column (GE Life Sciences) pre-equilibrated with NMR buffer (10 mM MES, pH 6.5 and 50 mM NaCl).

All of the bacterial expression constructs for human cyclophilins were previously described (Davis et al., 2010). Where possible, full-length proteins were expressed. However, isolated isomerase domains were expressed from the large, multidomain cyclophilins PPWD, PPIG, CWC27 due to solubility issues expressing full-length proteins. PPIH, PPIL3 and PPIG were cloned into the pET22b-based parallel vector system (Sheffield et al., 1999) with TEV-cleavable tags; PPIH and PPIL3 had a His_6GST tag to enhance yield and stability, and PPIG had a His_6 tag.

Rosetta (DE3) cells containing cyclophilin expression plasmids were grown at 37°C in LB with appropriate antibiotics until they reached OD_{600} 0.8-1. Expression was induced with 0.5 mM IPTG and then the growth was continued overnight at 16°C. Cells were resuspended in Buffer A, lysed in a cell disruptor, and then purified by Ni-NTA column according to manufacturer's protocol (QIAGEN). Tags were not cleaved with the exception of His_6GST-PPIH, which was subjected to overnight incubation with His_6-TEV protease at 4°C. The cleaved His_6GST tag was removed by passing the sample over Ni/NTA resin. All cyclophilins were further purified by running on a preparative grade Superdex 75 16/600 size-exclusion column pre-equilibrated with 20 mM HEPES pH 7.0, 100 mM NaCl, and 2 mM TCEP. For His_6GST-PPIL3, the fusion protein tag was not cleaved and the pH was increased to pH 7.5 to increase stability of the purified protein at room temperature.

Using the baculovirus expression system (Invitrogen), the His_6-tagged photolyase homology region (PHR, residues 1-491) of mouse CRY1 was expressed in Sf9 suspension insect cells (Expression Systems). Cells were infected with a high titer P3 virus at 1.5×10^6 cells/mL and grown for 72 hr with gentle shaking at 27°C. Following brief centrifugation at 4,000 rpm, cells were resuspended in 50 mM Tris pH 7.5, 200 mM NaCl, 20 mM imidazole, 10% (vol/vol) glycerol, 0.2% (vol/vol) Triton X-100, 0.1% (vol/vol) NP40, 0.4% (vol/vol) Tween-20, 5 mM β-mercaptoethanol and 1X EDTA-free protease inhibitors (Pierce). Cells were lysed using a cell disruptor followed by brief sonication on ice with a ¼ inch probe (3 pulses of 15 s. on/30 s. off). Lysate was clarified by centrifugation at 37,000 rpm at 4°C for 1 hr. His_6-CRY1 protein was isolated by Ni-NTA agarose affinity chromatography, and then further purified by size-exclusion chromatography on a preparative grade Superdex 200 16/600 column (GE Life Sciences) pre-equilibrated with 20 mM HEPES pH 7.5, 125 mM NaCl, 5% (vol/vol) glycerol and 2 mM TCEP. Prior to fluorescence anisotropy experiments, all purified proteins were buffer exchanged into assay buffer: 50 mM Bis-Tris Propane, 100 mM NaCl, 2 mM TCEP and 0.05% (vol/vol) Tween-20.

Peptide synthesis and purification

8-mer switch peptides DFSDLPWPL, FSDLPWPL, FSDLPAPL, FSDLPWAL were synthesized by solid phase peptide synthesis on 3-chlortrityl resin with standard Fmoc chemistry. One or two 1:4:4:4:6 molar ratio of resin:HBTU:HOAT:Fmoc-AA-OH:DiPEA coupling reactions were performed in DMF for each amino acid addition. The *cis*-locked peptide FSDLPWdmPL (dmP,

5,5-dimethyl L-proline) was synthesized by solid phase peptide synthesis using standard Fmoc chemistry. Coupling of dmP onto the Leu-Resin was performed using 1:2:2:4 molar ratio of Resin:HATU:Fmoc-dmP-OH:DiPEA, and coupling of the Trp onto the Resin-Leu-dmP was performed using 1:3.8:4:6 molar ratio of Rsin:COMU:Fmoc-Trp-Boc-OH:DiPEA; all other coupling reactions were performed using HBTU/HOAT as described above. Naturally occurring Fmoc-protected amino acids were purchased from Fluka, Nova Biochem, AAPPTec, or Sigma Aldrich. Fmoc-dmP was purchased from PolyPeptide Group (Cat. # FA21702). Peptides were purified by reverse phase C18 HPLC; purity (> 90%) and identity were verified by MS/MS on a Waters HPLC-MS/MS system.

The BMAL1 short TAD (residues 594-626) containing the P625dmP mutation and 8-mer switch peptides FSDLPFPL, FSDLPYPL and the insect BMAL1 peptide FSGLPWPLP were purchased from Bio-Synthesis. The mouse CRY1 CC peptide (residues 471-503) was synthesized and purified as described previously (Xu et al., 2015).

Mass spectrometry

The ^{15}N BMAL1 TAD NMR sample was separated by a Surveyor HPLC system (Thermo Finnegan) with the Proto 300 C4 reverse-phase column (Higgins Analytical) with 5 μm particle size. A 20 μL aliquot of the sample was injected at flow rate of 200 μL/min with an autosampler tray at a temperature setting of 4°C. The mobile phase consisted of solvent A: 0.1% formic acid in HPLC-grade water and Solvent B: 0.1% formic acid in acetonitrile with the following gradient: time (t) = 0 to 3 min 95% solvent A and 5% solvent B; t = 28 min, 35% A and 65% B; t = 28.01 to 30 min, 5% A and 95% B; T = 30.01 to 40 min, 95% A and 5% B. The sample was then analyzed using a linear ion trap LTQ mass spectrometer system (Thermo Finnegan). Proteins were detected by full scan MS mode (over the m/z 300-3000) in positive mode. The electrospray voltage was set to 5 kV. Mass measurements of deconvoluted ESI mass spectra of the reversed-phase peaks were generated by Magtran software (Zhang and Marshall, 1998).

NMR spectroscopy

NMR experiments were conducted on a Varian INOVA 600-MHz spectrometer equipped with ^{1}H, ^{13}C, ^{15}N triple resonance, Z axis pulsed field gradient cryoprobe. Sample temperatures were calibrated with the use of an ethylene glycol standard supplied by Agilent. At each temperature, NMR samples were given a 30 min equilibration time prior to calibration and data acquisition. All NMR data were processed using NMRPipe/NMRDraw (Delaglio et al., 1995). Chemical shift assignment of mBMAL1 TAD was previously reported (Xu et al., 2015). ^{15}N-^{1}H HSQC titrations of BMAL1 TAD were performed in a 300 μL volume of 100 μM ^{15}N BMAL1 TAD in NMR buffer (10 mM MES pH 6.5, 50 mM NaCl) with 10% (vol/vol) D_2O by stepwise addition of CBP KIX or CRY1 CC peptide, followed by concentration in an Amicon Ultra centrifugal filter with a 3 kDa molecular weight cutoff. All titration data were collected at 25°C. Titration data were analyzed with NMRViewJ (One Moon Scientific) using chemical shift perturbations defined by the equation $\Delta\delta_{TOT} = [(\Delta\delta^{1}H)^2 + (\chi(\Delta\delta^{15}N)^{2]1/2}$ and normalized with the scaling factor $\chi = 0.5$ (Johnson, 2004).

^{15}N-^{1}H ZZ-exchange experiments (Farrow et al., 1994) were collected on 400 μM ^{15}N BMAL1 TAD in NMR buffer (10 mM MES pH 6.5, 50 mM NaCl) with 10% (vol/vol) D_2O with 24 interleaved mixing times ranging from 0-3 s (0, 0.05, 0.1, 0.25, 0.5, 0.75, 1,1.25, 1,5, 1.75, 2, 2.5, 3) at temperatures of 25, 35, 45, 55, 60 and 65°C. Integration of the auto and cross peak intensities for each mixing time were extracted using NMRViewJ (One Moon Scientific). Cross peak intensities were normalized to the nominal cross peak intensities at time t = 0, and total intensity was set to the sum of the integrations of the *cis* and *trans* peaks at t = 0. The exchange constant k_{ex} was calculated by fitting integration data to an exchange model for two-state interconversion as described by Equations 1, 2, 3, and 4 (Kleckner and Foster, 2011; Palmer et al., 2001) using MATLAB (MathWorks):

$$I_{AA}(T) = \frac{1}{2}P_A\left(\frac{(1 - R^0_{1A} - R^0_{1B} + k_{ex}(\rho_B - \rho_A))}{\lambda_+ - \lambda_-}\right)e^{-\lambda_- t} + \left(1 + \left(\frac{(1 - R^0_{1A} - R^0_{1B} + k_{ex}(\rho_B - \rho_A))}{\lambda_+ - \lambda_-}\right)e^{-\lambda_= t}\right) \quad \text{(Equation 1)}$$

$$I_{BB}(T) = \frac{1}{2}P_B\left(\frac{(1 - R^0_{1A} - R^0_{1B} + k_{ex}(\rho_B - \rho_A))}{\lambda_+ - \lambda_-}\right)e^{-\lambda_- t} + \left(1 + \left(\frac{(1 - R^0_{1A} - R^0_{1B} + k_{ex}(\rho_B - \rho_A))}{\lambda_+ - \lambda_-}\right)e^{-\lambda_= t}\right) \quad \text{(Equation 2)}$$

$$I_{AB}(T) = P_B\left(\frac{(k_{ex}P_A)}{\lambda_+ - \lambda_-}\right)\left(e^{-\lambda_- t} - e^{-\lambda_= t}\right) \quad \text{(Equation 3)}$$

$$I_{BA}(T) = P_{BA}\left(\frac{(k_{ex}P_B)}{\lambda_+ - \lambda_-}\right)\left(e^{-\lambda_- t} - e^{-\lambda_= t}\right). \quad \text{(Equation 4)}$$

I refers to the time dependence of the transfer amplitudes (represented by the build-up curves) for the *cis* (AA), *trans* (BB) and *trans* to *cis* (BA), and *cis* to *trans* (AB) interconversions. *P* refers to the population of the indicated state, k_{ex} is the stochastic exchange of molecules between the two states per second, t is time in seconds, T is temperature in Kelvin, and R1A and R1B are the longitudinal relaxation rate constants in the absence of exchange.

The interconversion rates of *cis* to *trans* (k_{-1}) and *trans* to *cis* (k_1) were calculated using the relative populations of the two isomers taken from the integrations using Equations 5, 6, and 7:

$$k_{ex} = k_1 + k_{-1} \quad \text{(Equation 5)}$$

$$k_1 = k_{ex} * P_{trans} \quad \text{(Equation 6)}$$

$$k_{-1} = k_{ex} * P_{cis}. \quad \text{(Equation 7)}$$

Rates of isomerization were extrapolated to 25°C and 37°C using the Eyring equation (Equation 8). The free energy of isomerization was calculated based on transition state theory using Equation 9 and the difference in free energy between the two isomers calculated using Equation 10:

$$ln\frac{K}{T} = -\frac{\Delta H}{RT} + ln\frac{k_B}{h} + \frac{\Delta S}{R} \quad \text{(Equation 8)}$$

$$\Delta G^{\neq} = -RTln\left(\frac{hK_{CT}}{k_B T}\right) \quad \text{(Equation 9)}$$

$$\Delta G = \left|\Delta G^{\neq}_{CT} - \Delta G^{\neq}_{TC}\right|. \quad \text{(Equation 10)}$$

T is temperature, R is the gas constant, k_B is the Boltzmann constant, h is Planck's constant, and ΔH and ΔS are the activation enthalpy and entropy, respectively, of *cis* to *trans* (CT) and *trans* to *cis* (TC) isomerization. The free energy of the isomerization was calculated using Equation 8.

To assess rate enhancement of interconversion by cyclophilins, ^{15}N-^{1}H ZZ-exchange data were collected on 400 μM ^{15}N BMAL1 TAD with 100 μM cyclophilin (natural abundance) in cyclophilin NMR buffer, 20 mM HEPES pH 7.0, 100 mM NaCl, and 2 mM TCEP with 10% (vol/vol) D_2O. As described above, the pH of the buffer was increased to pH 7.5 for His_6GST-PPIL3 to increase stability of the purified protein at room temperature. ZZ data were collected as above, except that experiments were performed at room temperature (22.68°C). The fold enhancement of isomerization rates was determined by comparing the uncatalyzed rates with catalyzed rates extrapolated to room temperature for the isolated BMAL1 TAD.

Fluorescence anisotropy

The BMAL1 short TAD WT, P625A, P625dmP and Δswitch (594-F619Y) probes were purchased from Bio-Synthesis with a 5,6-TAMRA fluorescent probe covalently attached to the N terminus. The C terminus of the Δswitch peptide was amidated, while the others were left as a free carboxyl group to mimic the native C-terminal group of the TAD at L626. Equilibrium binding assays with CRY1 PHR were performed in 50 mM Bis-Tris Propane pH 7.5, 100 mM NaCl, 2 mM TCEP and 0.05% (vol/vol) Tween-20. With CBP KIX, the assay was performed in 10 mM MES, pH 6.5, 50 mM NaCl and 0.05% (vol/vol) Tween-20. Concentrated stocks of BMAL1 TAD probes were stored between 15-200 μM at −70°C and diluted into assay buffer to 50 nM alone and in the presence of increasing concentrations of test proteins. Plates were incubated at room temperature for 10-20 min prior to analysis. Binding was monitored by changes in fluorescence polarization with an EnVision 2103 multilabel plate reader (Perkin Elmer) with excitation at 531 nm and emission at 595 nm. The Hill coefficient (n_H) and equilibrium binding dissociation constant (K_D) were calculated by fitting the dose-dependent change in millipolarization (Δmp) to a one-site specific binding model in Prism 6.0 (GraphPad), with averaged Δmp values from duplicate or triplicate assays. Data shown are from a representative experiment (n = 4 replicates) of three independent assays.

Isothermal titration calorimetry

ITC measurements were obtained as previously described (Xu et al., 2015). Briefly, proteins were extensively dialyzed at 4°C in 10 mM MES pH 6.5, 50 mM NaCl using a 2 kDa molecular cutoff filter dialysis tubing (Spectrum Labs) prior to collecting ITC data. ITC was performed on a MicroCal VP-ITC calorimeter at 25°C with a stir speed of 177 rpm, reference power of 10 μCal/sec and 10 μL injection sizes. Protein ratios for the cell and syringe for the ITC assays (3 independent runs for each complex) were 220-230 μM CBP KIX titrated into 20-25 μM BMAL1 TAD WT, P625A, or P625dmP (N = 0.6-0.9). All data were best fit by a one-site binding model using Origin software.

QUANTIFICATION AND STATISTICAL ANALYSIS

Where applicable, statistical parameters including sample size, precision measures (standard deviation, s.d.) and statistical significance are reported in the Figures and corresponding Figure Legends.

Cellular Period Analysis

A LumiCycle luminometer (Actimetrics) was used to monitor luminescence (in counts/sec) as a function of time, and data were analyzed using the LumiCycle Analysis program (version 2.54, Actimetrics). The first 24 hr of recording were omitted from data processing, and then the raw data were baseline corrected and fit to a damped sine wave, from which period length, goodness of fit, amplitude and damping rate were determined. Data were deemed acceptable if the goodness of fit exceeded 80%. For *Bmal1*$^{-/-}$*;Per2*^{Luc} cells, at least two dishes per clonal line were tested for each run with four repeats (n = 8-12). The mean trace of all recordings with s.d. is reported. Statistical significance between genotypes or drug treatments was assessed using an unpaired t test in Prism 6.0.

Analysis of *cis*/trans isomerization rates

Experimentally determined rate constants for isomerization were visualized on an Eyring plot with representative s.d. errors from the derivation of individual *cis-trans* and *trans-cis* exchange rates from the time series NMR data. Data points at 55°C, 60°C, and 65°C were fitted to a linear regression to extrapolate exchange rates, not fast enough to detect experimentally by NMR, at lower temperatures (e.g., 25°C and 37°C).

DATA AND SOFTWARE AVAILABILITY

Raw data from the following ^{15}N-^{1}H ZZ exchange NMR time series experiments on ^{15}N BMAL1 TAD are available at Mendeley Data:

- 25°C time series: http://dx.doi.org/10.17632/4hs472w6wb.1
- 55°C time series: http://dx.doi.org/10.17632/8yx9wzt9gh.1
- 60°C time series: http://dx.doi.org/10.17632/gjfjvjpvdr.1
- 65°C time series: http://dx.doi.org/10.17632/kn58vc7hww.1
- room temperature time series with PPIA: http://dx.doi.org/10.17632/4txk4b3w5g.1
- room temperature time series with PPIE: http://dx.doi.org/10.17632/pt8xjvjs2v.1
- room temperature time series with PPIF: http://dx.doi.org/10.17632/x8yn6x28x8.1
- room temperature time series with PPIG: http://dx.doi.org/10.17632/fh595ry88h.1
- room temperature time series with PPIH: http://dx.doi.org/10.17632/mpykzm4kw2.1
- room temperature time series with PPIL1: http://dx.doi.org/10.17632/f9fxfynfrb.1
- room temperature time series with PPIL2: http://dx.doi.org/10.17632/cg8fb64p5f.1
- room temperature time series with PPIL3: http://dx.doi.org/10.17632/fmhg69tcxf.1
- room temperature time series with PPWD: http://dx.doi.org/10.17632/csc3c5hs32.1
- room temperature time series with CWC27: http://dx.doi.org/10.17632/htvhkdt7rw.1

An algorithm for analysis of ZZ exchange NMR time series data (and instructions for its use in MATLAB) are available at Mendeley Data at http://dx.doi.org/10.17632/w7ytgp2y9d.1.

Molecular Cell, Volume *66*

Supplemental Information

A Slow Conformational Switch in the BMAL1 Transactivation Domain Modulates Circadian Rhythms

Chelsea L. Gustafson, Nicole C. Parsley, Hande Asimgil, Hsiau-Wei Lee, Christopher Ahlbach, Alicia K. Michael, Haiyan Xu, Owen L. Williams, Tara L. Davis, Andrew C. Liu, and Carrie L. Partch

List of Supplemental Information

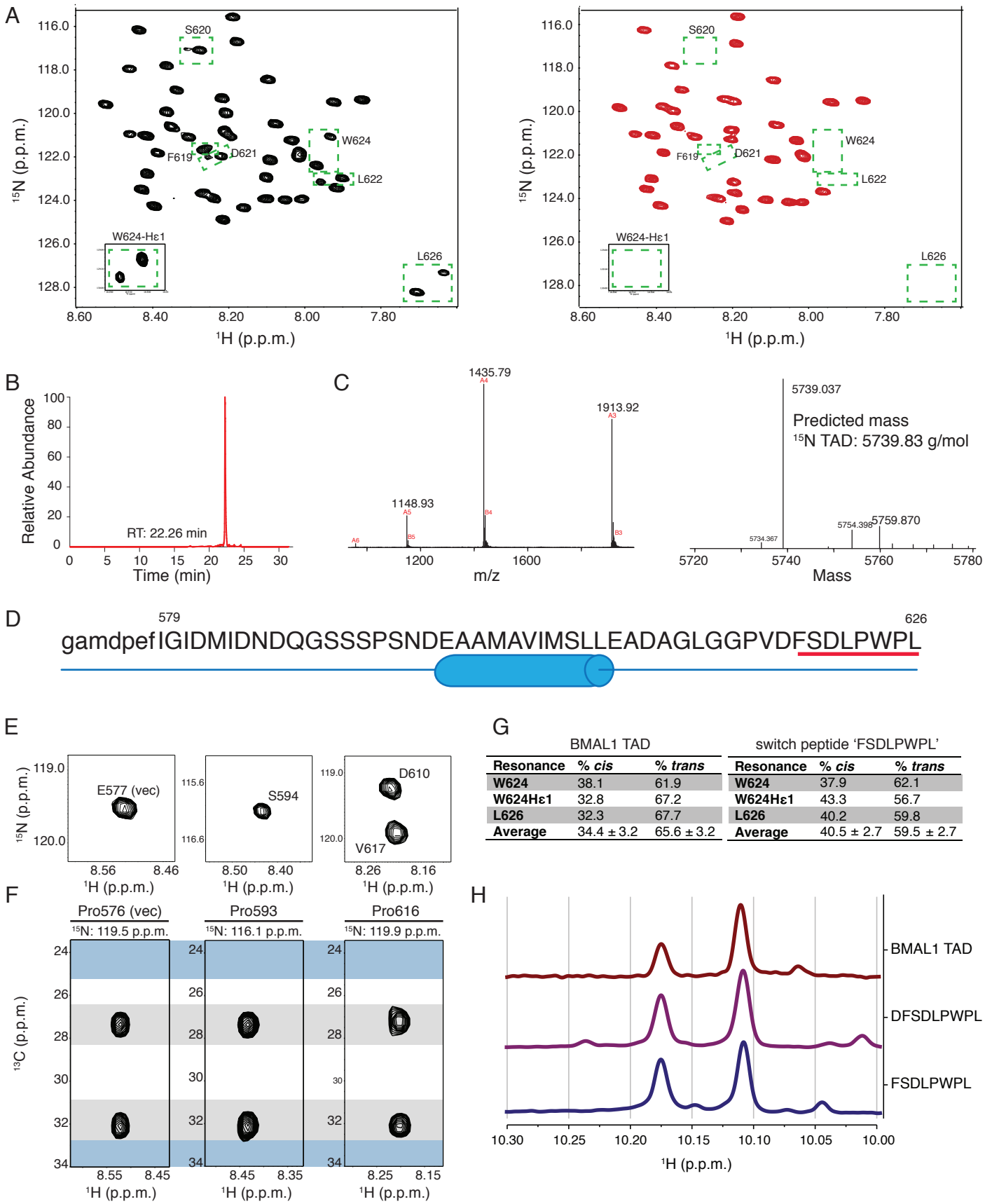

G

BMAL1 TAD			switch peptide 'FSDLPWPL'		
Resonance	**% *cis***	**% *trans***	**Resonance**	**% *cis***	**% *trans***
W624	38.1	61.9	**W624**	37.9	62.1
W624Hε1	32.8	67.2	**W624Hε1**	43.3	56.7
L626	32.3	67.7	**L626**	40.2	59.8
Average	34.4 ± 3.2	65.6 ± 3.2	**Average**	40.5 ± 2.7	59.5 ± 2.7

Figure S1

Figure S1: Identification of the BMAL1 TAD switch. Related to Figure 1
(A) ^{15}N-^{1}H HSQC of WT BMAL1 TAD (579-626) (left) and Δswitch BMAL1 TAD (579-619) (right) with green boxes indicating location of peak doubling. (B) HPLC trace of ^{15}N BMAL1 TAD following elution from a C4 reverse phase column. RT, retention time. (C) Initial mass spectrum of ^{15}N BMAL1 TAD (left) with deconvolution (right). (D) Primary sequence of BMAL1 TAD with the N-terminal vector sequence remaining after TEV cleavage indicated in lower case letters. Location of the predicted α-helical region is indicated below the sequence. Residues for which peak doubling was observed are underlined in red. (E) Regions of ^{15}N-^{1}H HSQC spectrum of the BMAL1 TAD displaying the backbone amide bond resonances for E577 (a vector artifact left after TEV cleavage; see (Xu et al., 2015) for details), S694, and V617, each of which are preceded by a proline. (F) Strips from the ^{13}C (H)C(CO)NH TOCSY spectrum of the BMAL1 TAD at the ^{1}H and ^{15}N chemical shifts corresponding to the backbone amides from E577, S564, and V617. Strips highlight the ^{13}C frequencies for P623 and P625 C_β and C_γ atoms (y-axis) with average ranges for ^{13}C frequencies observed for *trans* (gray) and *cis* (blue) isomers from (Shen and Bax, 2010). (G) Ratios of *cis* and *trans* isomers in ^{15}N BMAL1 TAD and the 8-mer WT switch peptide calculated from the peak volumes of the indicated residues ± s.d. (H) ^{1}H 1D spectra of the W624 indole region taken from natural abundance 8-mer WT switch peptides FSDLPWPL or the 9-mer DFSDLPWPL compared to the intact BMAL1 TAD (residues 579-626).

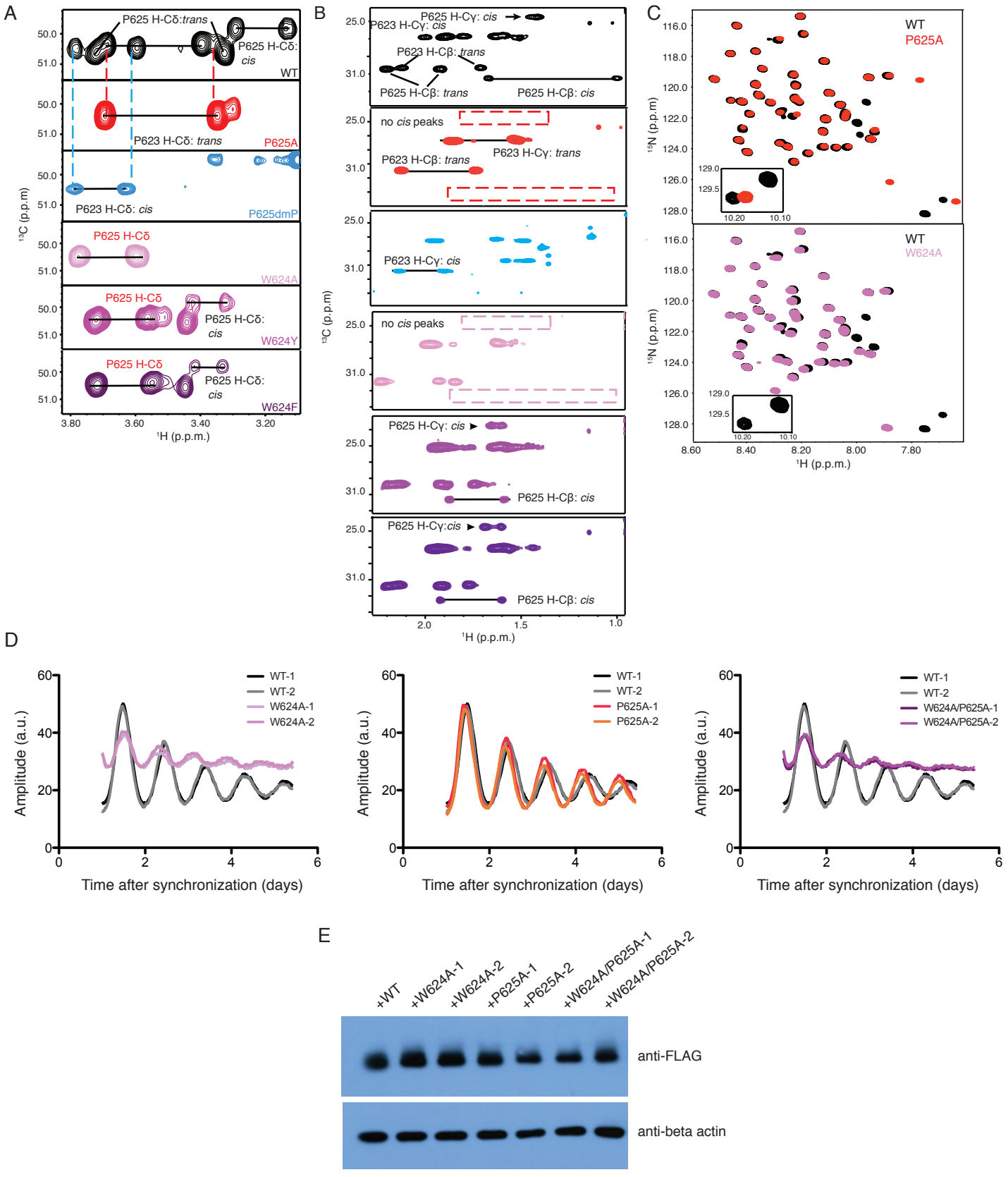
A
P625 H-Cδ:trans
P625 H-Cδ: cis
WT
P623 H-Cδ: trans
P625A
P623 H-Cδ: cis
P625dmP
P625 H-Cδ
W624A
P625 H-Cδ
P625 H-Cδ: cis
W624Y
P625 H-Cδ
P625 H-Cδ: cis
W624F
13C (p.p.m)
1H (p.p.m.)
B
P625 H-Cγ: cis
P623 H-Cγ: cis
P623 H-Cβ: trans
P625 H-Cβ: trans
P625 H-Cβ: cis
no cis peaks
P623 H-Cγ: trans
P623 H-Cβ: trans
P623 H-Cγ: cis
no cis peaks
P625 H-Cγ: cis
P625 H-Cβ: cis
P625 H-Cγ:cis
P625 H-Cβ: cis
13C (p.p.m)
1H (p.p.m.)
C
WT
P625A
WT
W624A
15N (p.p.m)
1H (p.p.m.)
D
WT-1
WT-2
W624A-1
W624A-2
P625A-1
P625A-2
W624A/P625A-1
W624A/P625A-2
Amplitude (a.u.)
Time after synchronization (days)
E
+WT
+W624A-1
+W624A-2
+P625A-1
+P625A-2
+W624A/P625A-1
+W624A/P625A-2
anti-FLAG
anti-beta actin

Figure S2

Figure S2: Assignment and cycling analysis of TAD switch mutants. Related to Figure 2

(A-B) Selected regions of ^{1}H-^{1}H TOCSY NMR spectra of the following TAD 8-mer peptides: WT TAD (FSDLPWPL, black); P625A (FSDLPWAL, red); P625dmP (FSDLPWdmPL, blue); W624A (FSDLPAPL; pink); W624F (FSDLPFPL, violet); and W624Y (FSDLPYPL, purple) showing the (A) Pro C_{δ} chemical shifts and (B) Pro C_{γ} and C_{β} chemical shifts. (C) ^{15}N-^{1}H HSQCs of the ^{15}N WT BMAL1 TAD (black) overlaid with ^{15}N BMAL1 TAD P625A (upper panel, red) or W624A (lower panel, pink) mutants. (D) Bioluminescence traces for individual clonal lines of WT, W624A, P625A, and W624A/P625A *Bmal1*-complemented *Bmal1*$^{-/-}$;*Per2*^{Luc} fibroblasts. (E) Western blot analysis of relative expression levels of FLAG-BMAL1 for WT, W624A, P625A, and W624A/P625A *Bmal1*-complemented *Bmal1*$^{-/-}$;*Per2*^{Luc} fibroblasts. Actin is shown as a loading control.

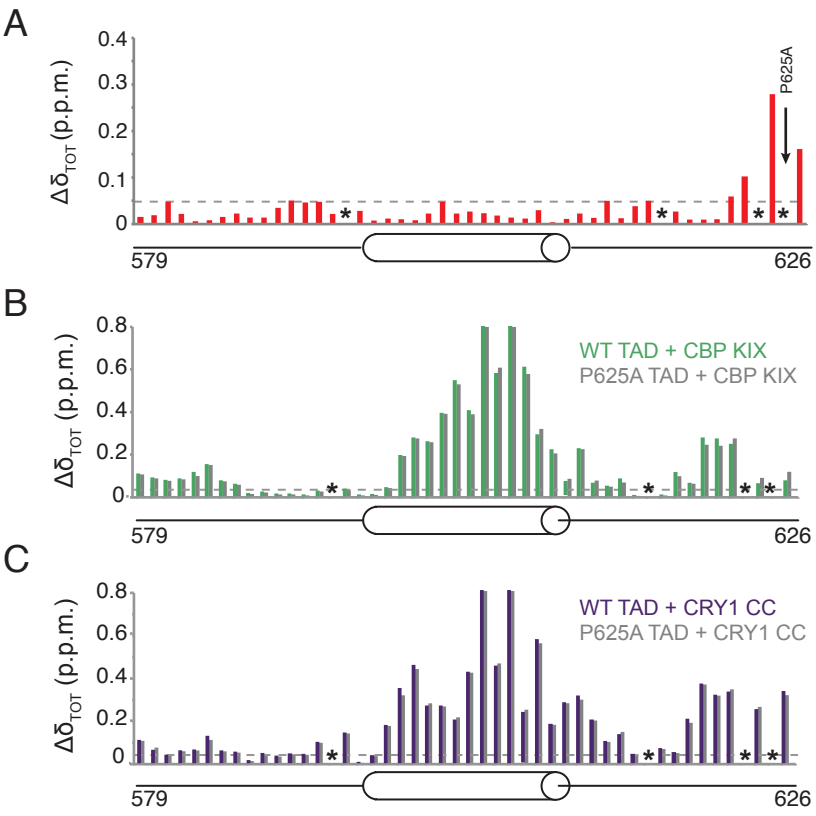

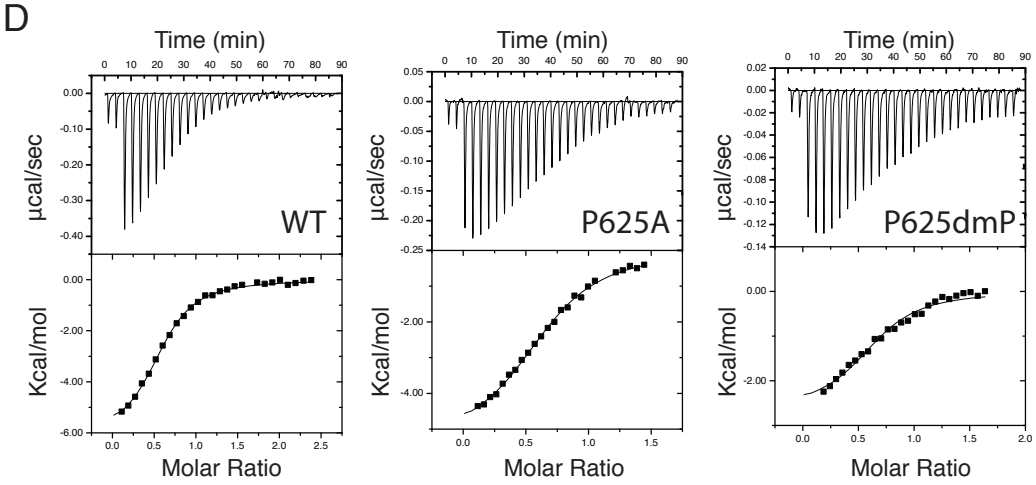

E

BMAL1 TAD	K_D (µM)
WT	2.78 ± 0.18
P625A	2.64 ± 0.49
P625dmP	2.59 ± 0.83

Figure S3

Figure S3: Quantitative analysis of conformationally locked BMAL1 TAD switch isomers with CRY1 and CBP KIX. Related to Figure 3

(A) Chemical shift analysis of ^{15}N-^{1}H HSQC spectra of ^{15}N WT BMAL1 TAD and the P625A mutant, represented as the total change in chemical shift ($\Delta\delta_{TOT}$) in parts per million (p.p.m.). Dashed line is the significance cutoff for chemical shift perturbation, set at 0.05 p.p.m. Residue numbering and the predicted secondary structure are illustrated below the plot, with the location of the mutant indicated by an arrow. Asterisks indicate location of prolines in the TAD sequence, for which there are no crosspeaks. (B) Chemical shift analysis of ^{15}N-^{1}H HSQC spectra of ^{15}N WT BMAL1 TAD (green) and the P625A mutant (gray) binding to the CBP KIX domain. (C) Chemical shift analysis of ^{15}N-^{1}H HSQC spectra of ^{15}N WT BMAL1 TAD (purple) and the P625A mutant (gray) binding to the CRY1 CC helix. (D) Binding isotherms from isothermal titration calorimetry (ITC) experiments of CBP KIX domain titrated into the short WT BMAL1 TAD (residues 594-626, left), P625A (middle) and P625dmP (right). All ITC experiments were set up with 15-30 μM BMAL1 TAD in the cell and 220-250 μM CBP KIX in the syringe and run at 25°C with 177 r.p.m. stir speed. (E) ITC data were fit to a one-site binding model in Origin software to derive affinities ± s.d. (n = 3) with representative N values of stoichiometry from 0.6-0.8.

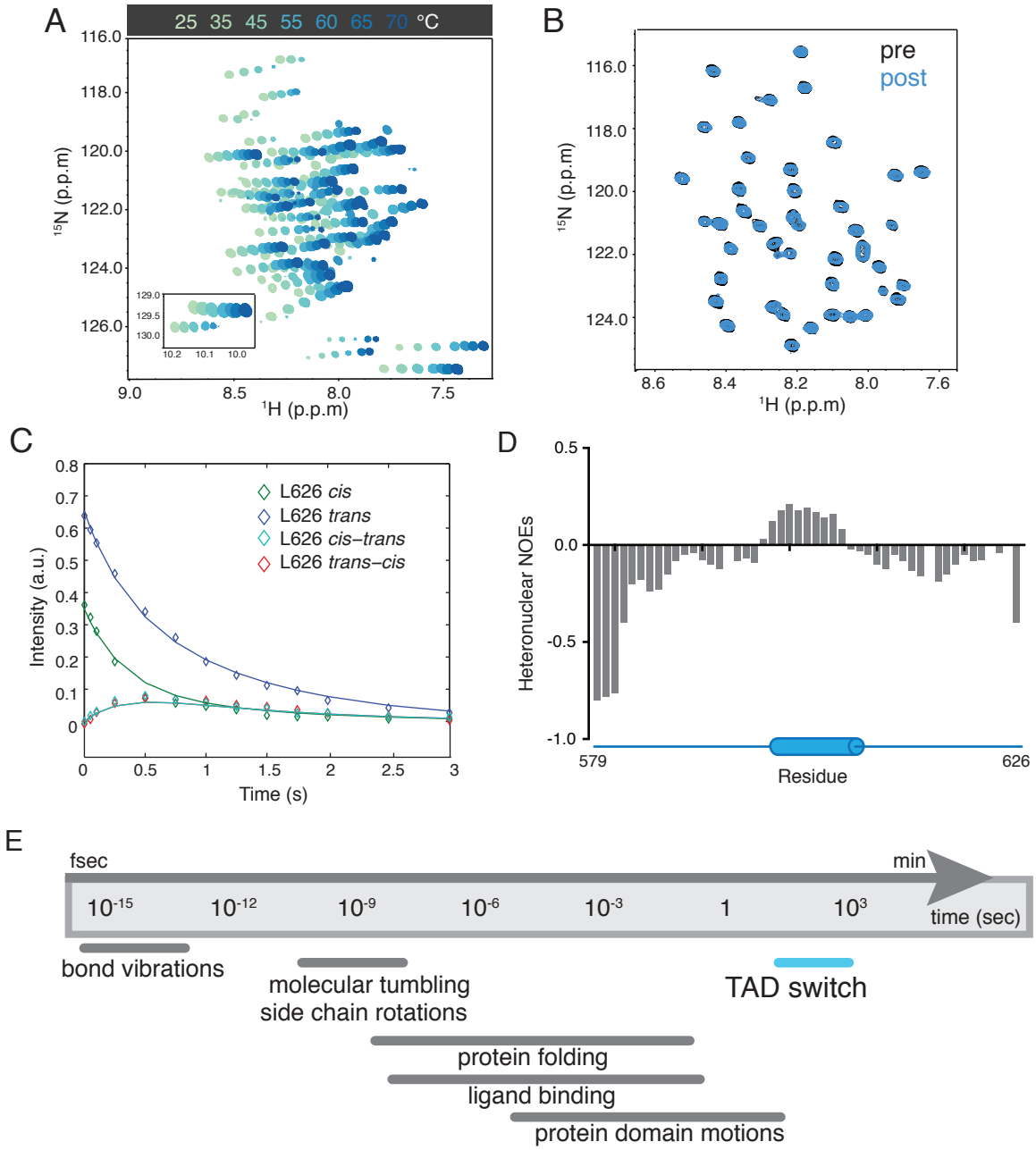
A
25 35 45 55 60 65 70 °C
116.0
118.0
120.0
122.0
124.0
126.0
^{15}N (p.p.m)
129.0
129.5
130.0
10.2 10.1 10.0
9.0 8.5 8.0 7.5
^{1}H (p.p.m)
B
pre
post
116.0
118.0
120.0
122.0
124.0
^{15}N (p.p.m)
8.6 8.4 8.2 8.0 7.6
^{1}H (p.p.m)
C
L626 cis
L626 trans
L626 cis–trans
L626 trans–cis
Intensity (a.u.)
0.8 0.7 0.6 0.5 0.4 0.3 0.2 0.1 0
0 0.5 1 1.5 2 2.5 3
Time (s)
D
Heteronuclear NOEs
0.5
0.0
-0.5
-1.0
579
626
Residue
E
fsec
min
10^{-15} 10^{-12} 10^{-9} 10^{-6} 10^{-3} 1 10^{3}
time (sec)
bond vibrations
molecular tumbling
side chain rotations
TAD switch
protein folding
ligand binding
protein domain motions

Figure S4

Figure S4: Analysis of *cis/trans* isomerization by NMR spectroscopy. Related to Figure 4

(A) Overlaid ^{15}N-^{1}H HSQC spectra of WT BMAL1 TAD at temperatures from 25-70°C. (B) Overlay of ^{15}N-^{1}H HSQC spectra of WT BMAL1 TAD at 25°C before and after acquisition of the temperature series up to 70°C. (C) A representative build-up curve from the ^{15}N-^{1}H ZZ exchange assay for L626 at 55°C generated by plotting peak intensities of the *cis*, *trans* and exchange cross peaks as a function of delay time. (D) ^{15}N-^{1}H heteronuclear NOE values as a function of primary sequence of the BMAL1 TAD. (E) A comparison of molecular motion timescales common to biomolecules relative to the slow motion of the BMAL1 TAD switch (adapted from (Henzler-Wildman and Kern, 2007)).

A

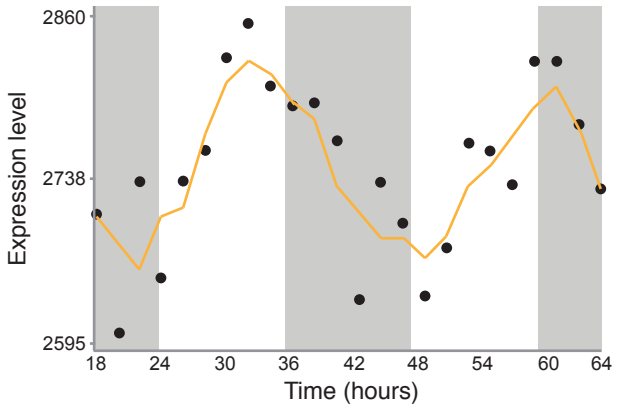

B

Gene	RefSeq DNA	Database	Probeset	JTK p-value	JTK q-value	Period	Phase
PPIF	NM_134084	Mouse Liver 1.OST	10413222	0.00000496	0.0003	26	16
		Mouse Liver 48 Hr Hughes '09	1438955_x_at	0.00035	0.0056	28	14.5
PPIA	NM_008907	Mouse Lung 1.OST	10588024	0.0023	0.036	26	11
		Mouse Lung 1.OST	10374175	0.00024	0.0074	26	11
		Mouse Cerebellum 1.OST	10588024	0.0000108	0.0074	26	10
		Mouse Cerebellum 1.OST	10374175	0.000046	0.0185	26	10
		Mouse Cerebellum 1.OST	10441396	0.000046	0.0185	28	10
		Mouse Cerebellum 1.OST	10545337	0.000236	0.042	26	9
PPIL1	NM_026845	Mouse Liver 1.OST	10449575	0.001	0.014	24	19
		Mouse Liver 48 Hr Hughes '09	1428892_at	0.0000183	0.00045	27	18.5
PPIH	NM_028677	Mouse Kidney 1.OST	10447702	0.00000616	0.00077	24	22
		Mouse Kidney 1.OST	10381526	0.0000132	0.0012	24	22
		Mouse Kidney 1.OST	10521690	0.000279	0.0099	24	22
		Mouse Aorta 1.OST	10381526	0.000046	0.0101	22	0
		Mouse Aorta 1.OST	10447702	0.000108	0.017	22	0
		Mouse Aorta 1.OST	10521690	0.00018	0.021	22	0

Figure S5

Figure S5, Circadian expression of select cyclophilin genes. Related to Figure 5

(A) Representative gene expression profile for PPIA in the mouse cerebellum from the Circadian Expression Profiles Data Base (CircaDB, http://bioinf.itmat.upenn.edu.circa), an open access site that analyzes and displays rhythmic gene expression from microarray and RNASeq datasets (Pizarro et al., 2013). Black dots, expression at individual time points. Yellow line, average expression. White and gray background, subjective day and night time, respectively. (B) Circadian gene expression parameters for cyclophilins tested for activity against the BMAL1 TAD *in vitro*. Database, original publication: Mouse 1.OST, RNASeq data (unpublished); Liver 48 Hr Hughes (GEO number GSE11923; Microarray) (Hughes et al., 2009). Cyclophilins with circadian expression were defined after analysis by JTK_Cycle with a p-value <0.05 and q-value (estimation of false discovery rate) < 0.1 for circadian time series data (Hughes et al., 2010).